AGU PUBLICATIONS

Radio Science

RESEARCH ARTICLE
10.1002/2013RS005230

Key Points:
- Microwave interferometric radiometers are new instruments
- The manuscript presents a historial review of the development of these
- The successful in-orbit demonstration of SMOS

Correspondence to:
M. Martín-Neira,
manuel.martin-neira@esa.int

Citation:
Martín-Neira, M., et al. (2014), Microwave interferometric radiometry in remote sensing: An invited historical review, *Radio Sci.*, *49*, 415–449, doi:10.1002/2013RS005230.

Received 14 MAY 2013
Accepted 7 APR 2014
Accepted article online 23 APR 2014
Published online 24 JUN 2014

Microwave interferometric radiometry in remote sensing: An invited historical review

M. Martín-Neira[1], D. M. LeVine[2], Y. Kerr[3], N. Skou[4], M. Peichl[5], A. Camps[6], I. Corbella[6], M. Hallikainen[7], J. Font[8], J. Wu[9], S. Mecklenburg[10], and M. Drusch[1]

[1]European Space Agency, ESTEC, Noordwijk, Netherlands, [2]NASA Goddard Space Flight Centre, Greenbelt, Maryland, USA, [3]Centre d'Etudes Spatiales de la Biosphère, Toulouse, France, [4]DTU Space, Technical University of Denmark, Copenhagen, Denmark, [5]DLR, Microwaves and Radar Institute, Oberpfaffenhofen, Germany, [6]Department of Signal Theory and Communications, Polythecnic University of Catalonia, Barcelona, Spain, [7]Department of Radio Science and Engineering, Aalto University, Espoo, Finland, [8]Institut de Ciències del Mar-CSIC and SMOS Barcelona Expert Centre, Barcelona, Spain, [9]National Space Science Center, Beijing, China, [10]European Space Agency, ESRIN, Roma, Italy

Abstract The launch of the Soil Moisture and Ocean Salinity (SMOS) mission on 2 November 2009 marked a milestone in remote sensing for it was the first time a radiometer capable of acquiring wide field of view images at every single snapshot, a unique feature of the synthetic aperture technique, made it to space. The technology behind such an achievement was developed, thanks to the effort of a community of researchers and engineers in different groups around the world. It was only because of their joint work that SMOS finally became a reality. The fact that the European Space Agency, together with CNES (Centre National d'Etudes Spatiales) and CDTI (Centro para el Desarrollo Tecnológico e Industrial), managed to get the project through should be considered a merit and a reward for that entire community. This paper is an invited historical review that, within a very limited number of pages, tries to provide insight into some of the developments which, one way or another, are imprinted in the name of SMOS.

1. Introduction

1.1. Foreword

This paper includes contributions, in chronological order (Figure 33) from sections 2 to 9, from some of the major researchers and engineers across the world who significantly contributed to the development of *microwave interferometric radiometry*, in particular at L band: D. LeVine (NASA), Y. Kerr (Centre National d'Etudes Spatiales (CNES)), N. Skou (Technical University of Denmark (DTU)), M. Peichl (Deutsches Zentrum für Luft- und Raumfahrt (DLR)), M. Martín-Neira (European Space Agency (ESA)), A. Camps (Polytechnic University of Catalonia (UPC)), I. Corbella (UPC), M. Hallikainen (Aalto University), and J. Wu (National Space Science Center (NSSC)). But not all key people are mentioned, even including the acknowledgment section where some additional important names have been added. Those contributions collected within the available pages bring a historical review as well as a description of the most important instruments which were built at several laboratories (Figure 33 illustrates the global time line of these developments). The emphasis of the paper is on the engineers and scientists who led to this novel remote sensing technique rather than on the companies which did an excellent job in realizing their ideas. The contribution from each group has been integrated within the paper with little editing, to bring to the reader the distinct perspective of each group. It is worth noting that before this achievement, no microwave radiometer was capable of producing images in a single snapshot; instead, they had to scan or push broom pencil beams across all pixels of the field of view before being able to produce an image. *Microwave interferometric radiometers* thus avoid the need of mechanical scanning or multiple antennas in push broom mode, an important issue in spaceborne instruments, especially in the low-frequency region of the microwave spectrum.

1.2. Microwave Interferometric Radiometry

Aperture synthesis is a technique which was developed in the field of radio astronomy, based on the Van Cittert-Zernike theorem [*Goodman*, 1985]. According to this theorem the spatial frequencies (or visibility function) of a brightness temperature image can be obtained by cross correlating the radiated electric field at the two end points of a baseline. The baseline, measured in wavelengths, gives directly the value of the

spatial frequency. By proper distribution of the collecting antennas, a sufficiently large spatial domain of the visibility function can be measured, and the image reconstructed through linear inversion techniques. During the development of Soil Moisture and Ocean Salinity (SMOS) it became clear that the Van Cittert-Zernike theorem was inconsistent with the Bosma theorem of microwave noise waves. This fact was apparent when enclosing a breadboard of the SMOS payload inside an electromagnetic compatibility chamber or when measuring the cosmic microwave background radiation from the cold sky. A careful formulation of the problem resulted in a fundamental modification of the visibility equation as it had always been used in radio astronomy. This result, called the Corbella equation, is a bridge between the two theorems. The fundamental equation obeyed by microwave interferometric radiometers according to *Corbella et al.* [2004] is

$$V_{ij}^{pq}(u,v) = \frac{1}{\sqrt{\Omega_i^p \Omega_j^q}} \iint_{\xi^2+\eta^2 \le 1} F_{n,i}^{\alpha,p}(\xi,\eta) F_{n,j}^{\beta,q*}(\xi,\eta) \frac{T_B^{\alpha\beta}(\xi,\eta) - \delta_{\alpha\beta} T_r}{\sqrt{1-\xi^2-\eta^2}} \widetilde{r}_{ij}\left(-\frac{u\xi + v\eta}{f_o}\right) e^{-j\,2\pi(u\xi+v\eta)}\, \mathrm{d}\xi\, \mathrm{d}\eta$$

where V is the visibility function (in Kelvin), p and q are the polarizations for each of the two receivers i and j involved in a particular baseline, (u,v) are the baseline lengths normalized to the wavelength $\lambda_o = c/f_o$ where f_o is the center frequency of the instrument (nominally $f_o = 1413.5$ MHz in SMOS), (ξ,η) are the direction cosines, Ω is the solid angle of the corresponding antenna and polarization, ${F_n}^{\alpha,p}$ is the normalized voltage antenna pattern in α polarization when p polarization is selected, ${T_B}^{\alpha\beta}$ the brightness temperature in $\alpha\beta$ polarization (when $\alpha \neq \beta$, then ${T_B}^{\alpha\beta}$ and ${T_B}^{\beta\alpha}$ correspond to two conjugate complex numbers whose real and imaginary parts are the third and fourth Stokes parameters), T_r is the receiver physical temperature (assumed the same for all receivers) when an isolator is used at the input, $\widetilde{r}_{ij}$ is the fringe-washing function [*Thompson et al.*, 2004], and $\delta_{\alpha\beta}$ is the Kronecker delta. The equation is written using Einstein summation convention for convenience, so that a summation has to be taken over α and β.

1.3. Scientific Motivation

Soil moisture (SM) and sea surface salinity (SSS) are variables in the Earth's water cycle that scientists require on a global scale for applications such as understanding ocean circulation and climate change as well as for weather and hydrological forecasting. The objectives of the SMOS mission were based on the scientific requirements for these applications as defined by potential users [*Kerr*, 1998]. The mission objectives were (a) to provide global volumetric SM estimates with an accuracy of 0.04 m^3/m^3 at a spatial resolution of 35–50 km and a temporal sampling of 1–3 days and (b) to provide global SSS estimates with an accuracy of 0.1 practical salinity scale units (psu) for a 10–30 day average for an open ocean area of 200–100 km, respectively.

The Microwave Imaging Radiometer using Aperture Synthesis (MIRAS) instrument on SMOS was designed to meet these requirements. In particular are the following:

1. The choice of wavelength

The choice to operate in the L band window at 1.413 GHz set aside for passive use only has a number of advantages for remote sensing of soil moisture and ocean salinity. In the case of soils, it is low enough in frequency to provide a strong response to water content and reasonable penetration of vegetation and is high enough in frequency to provide reasonable resolution with a feasible antenna size. In the case of the oceans, it is near the peak response to salinity [*Le Vine et al.*, 2010] and the window at 1.413 GHz is the largest piece of spectrum (by far) protected for passive use. The latter is critically important for remote sensing of salinity because high radiometric sensitivity is required to achieve accuracy on the order of 0.1 psu (the sensitivity to changes in salinity is on the order of 0.5 K/psu).

2. Temporal revisit time

For land and in particular hydrological applications, the temporal revisit time is of high importance. Repeat coverage in 3 days or less requires a large field of view. Interferometry (aperture synthesis) as employed by MIRAS is an advantage in this case because it provides a wide field of view without requiring a scanning (i.e., moving) antenna.

3. Multiangular viewing

MIRAS observes each point in the footprint several times at varying incidence angles as the instrument advances in its orbit. The multiangular viewing provides additional information (i.e., independent views

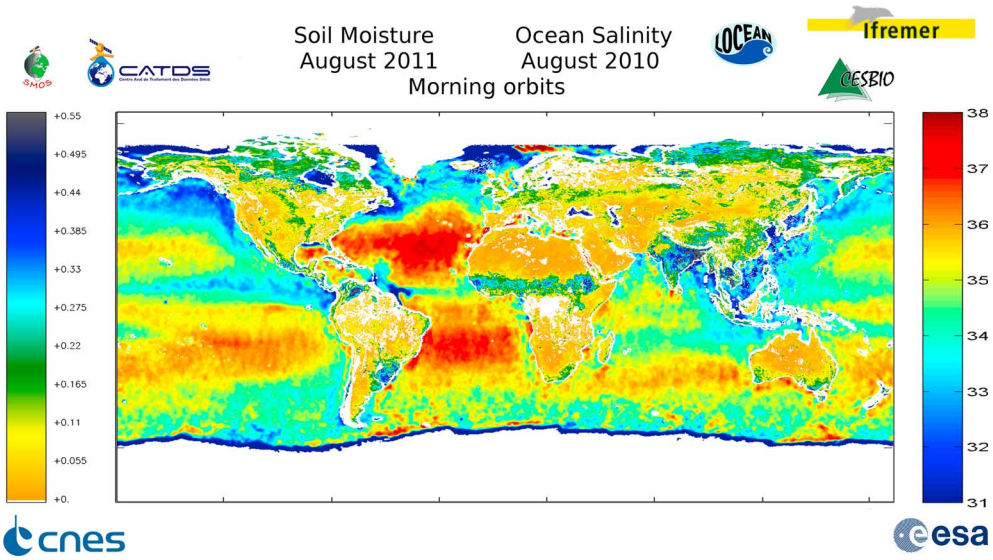

Figure 1. Soil Moisture and Ocean Salinity Global Map from SMOS (ascending orbits, August 210; left scale is SM volumetric fraction; right scale is SSS in practical salinity units)—courtesy of CESBIO, CATS, IFREMER, and LOCEAN.

ofthe same scene) which can be used to measure additional variables such as opacity of the vegetation canopy over land or surface roughness (waves) over the ocean. In the case of the soil moisture and ocean salinity retrievals, this is done using an iterative approach, minimizing a cost function between the observed and the modeled (i.e., theoretical) brightness temperatures [*Kerr et al.*, 2010; *Zine et al.*, 2008].

4. Polarimetric observations

MIRAS can be operated in dual or full polarization mode (always using linear polarization). The full polarization mode, in which the complete Stokes vector can be measured, requires more time, and consequently, a penalty is paid in radiometric noise. However, full-pol observations at L band are new. During the 6 months commissioning phase SMOS was operated in both polarization modes to test the respective capabilities, and at the end of the commissioning phase the decision was taken to operate MIRAS in the full polarization mode. The goals were to (a) provide a new type of observation (full polarimetric observations) not previously available at L band; (b) provide a direct, in situ measurement of Faraday rotation [*Yueh*, 2000], with the potential to improve level 2 SSS retrieval accuracy; and (c) examine the usefulness of third and fourth Stokes parameters to detect radio frequency interference (RFI) which has turned out to be a major source of degradation of SMOS data quality [*Daganzo et al.*, 2013].

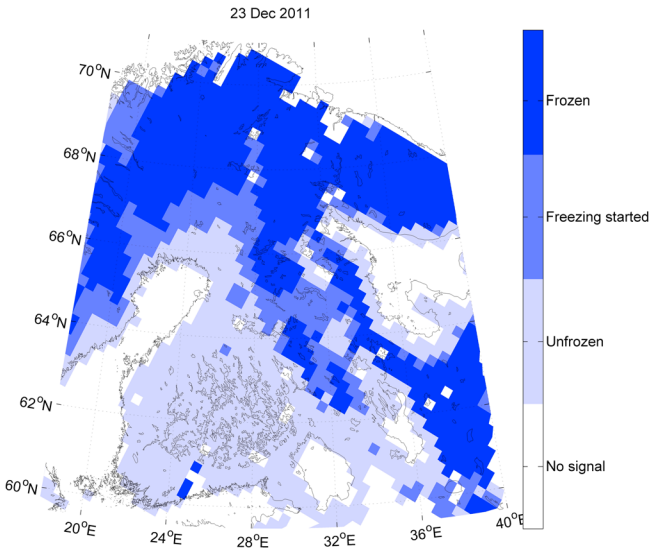

Figure 2. Depth of frozen soil in Finland estimated from SMOS data—courtesy Finnish Meteorological Institute.

SMOS has been operating successfully since its launch in November 2009, and global maps of SM and SSS are now routinely being retrieved (Figure 1). The novel information on SM can be used to improve the predictive skill of hydrological flood forecasting models, numerical weather prediction, and drought forecasting systems. Other information that can be derived from the observed brightness temperatures are freeze and thaw state and soil frost depth (Figure 2), sea ice thickness (Figure 3), and hurricane tracking (Figure 4).

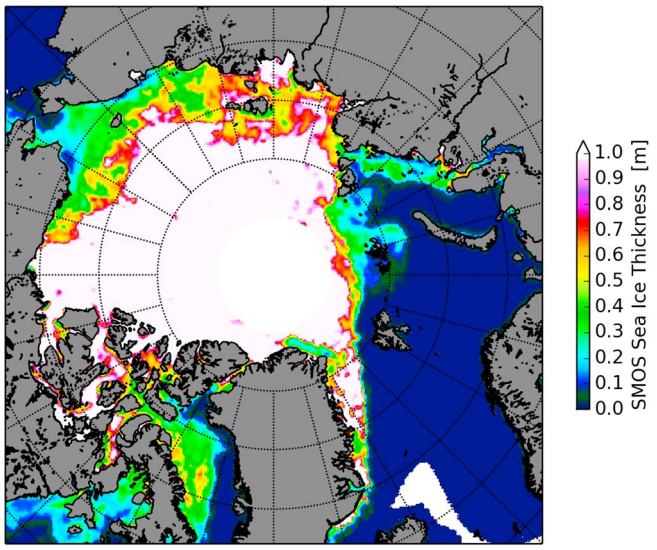

Figure 3. Sea ice thickness derived from SMOS—courtesy Hamburg University.

2. Development at the Goddard Space Flight Center: ESTAR and 2D-STAR

2.1. Introduction

Electronically Steered Thinned Array Radiometer (ESTAR) is an L band radiometer that employs aperture synthesis to obtain resolution in the across-track dimension and uses the "real" antenna aperture for resolution along track. It was developed at the Goddard Space Flight Center (GSFC) and the University of Massachusetts as an aircraft prototype to demonstrate the technology of aperture synthesis for remote sensing of the Earth from space. The theory was mature early in the 1980s [*Le Vine and Good*, 1983], but it was the teaming with C. Swift and his students at the University of Massachusetts that resulted in the realization of an actual instrument. The success of ESTAR in demonstrating the potential of aperture synthesis in one dimension for remote sensing led to proposals at GSFC for L band instruments in space, the most mature of which was called HYDROSTAR. ESTAR eventually was replaced by the two-dimensional synthetic aperture radiometer (2D-STAR) which employs aperture synthesis in both dimensions, but HYDROSTAR was never launched.

ESTAR employs "stick" antennas to achieve resolution along track and uses the correlation between sticks (aperture synthesis) to achieve resolution across track [*Le Vine et al.*, 1994]. ESTAR has five sticks oriented with their long axis in the direction of motion. Each stick antenna consists of an array (row) of eight horizontally polarized dipoles. The stick antennas are spaced at integer multiples of a half wavelength (about 10.5 cm) with a maximum spacing of $7\lambda/2$. With this configuration it is possible to obtain seven unique baselines plus one at the zero spacing. The result is a synthesized beam with a width of about ±4° at nadir in the cross-track dimension.

Figure 5 shows the antenna array with the radome removed. The antenna is mounted on the Earth-viewing side of a box containing the RF hardware. The signal from the antenna is amplified and mixed to IF inside the box and then sent to the correlator which is located in the aircraft cabin together with the computer controller, power supplies, and data storage [*Le Vine et al.*, 1994]. Over the course of the lifetime of ESTAR, many changes were made to both the RF electronics and the correlator [*Le Vine et al.*, 2001a, 2001b]. The most significant change to the electronics was to improve thermal control which had been limiting performance. The correlator technology in ESTAR remained analog but was changed to digital in the follow-on instrument, 2D-STAR.

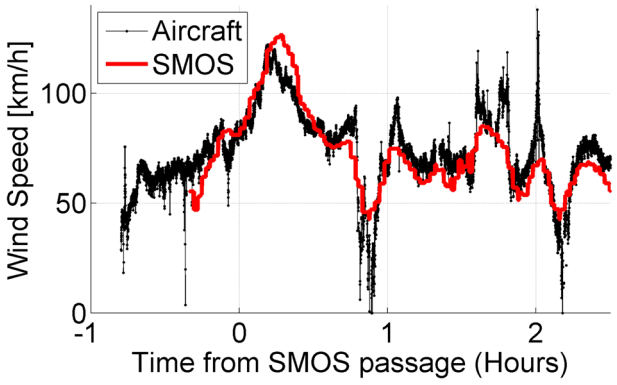

Figure 4. Hurricane wind speed estimation using SMOS brightness temperature—courtesy of IFREMER.

The principles of image reconstruction and calibration developed for ESTAR are outlined in *Le Vine et al.* [1994, 2001a, 2001b]. Novel features of the instrument at the time of its development include the implementation of the zero-spacing measurement using a noise injection radiometer that employed the correlator electronics [*Le Vine et al.*, 1994, Figure 5], and the image reconstruction using oversampled values of the impulse response and a pseudoinverse of the resultant matrix

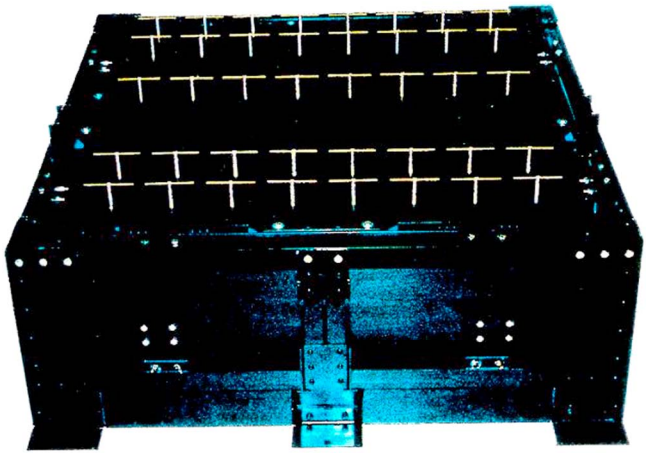

Figure 5. The ESTAR antenna array and RF box [*Le Vine and Good*, 1983].

("G" matrix [*Le Vine et al.*, 1994]). The latter (i.e., G matrix approach) was adopted in subsequent instrument and is used in SMOS, but the implementation of the noise injection radiometer used in ESTAR was not used in subsequent instruments. An important step in determining the impulse response during calibration was using the difference from a point noise source with signal on and signal off while in the anechoic chamber at GSFC. To a good first approximation, signal off amounted to looking at a scene with constant temperature (the walls of the anechoic chamber).

2.2. Experience With ESTAR

First images were reported in 1990 [*Le Vine et al.*, 1990] over a section of the Delmarva Peninsula close to Goddard's Wallops Flight Facility where tests of the hardware were performed. Figure 6 is a composite of data collected in this area showing ESTAR brightness temperature superimposed on a map of the region [*Swift et al.*, 1991]. One of the first "surprises" during these flights was the appearance of RFI in what is a band of the spectrum protected for passive use only [*Le Vine and Haken*, 2003]. Airports were identified as one source of RFI (presumably out-of-band emissions from air-traffic-control radar), but many sources were not identified.

ESTAR participated in several field experiments to measure soil moisture. Notable were the flights at the Walnut Gulch Watershed in 1991 [*Le Vine et al.*, 1994; *Jackson et al.*, 1993] which demonstrated the response of the instrument to changes in soil moisture and its ability to produce data of high scientific quality and as good as conventional L band radiometers of that era (e.g., the Push Broom Microwave Radiometer [*Jackson et al.*, 1993]). ESTAR supported soil moisture field campaigns at the Little Washita River Watershed in 1992 [*Jackson et al.*, 1995] and 1994, and later during the Southern Great Plains experiments in 1997 [*Jackson et al.*, 1999] and 1999 [*Le Vine et al.*, 2001a, 2001b]. In one sense, these experiments were technology demonstrations, showing that aperture synthesis for radiometers was viable for remote sensing of the Earth, but the experiments also produced data to support the value of using L band for future remote sensing of soil moisture from space. During this time, experiments were also conducted on remote sensing of sea surface salinity. These include the Delaware Coastal Current Experiment [*Le Vine et al.*, 1988] and an experiment called the "Gulf Stream Experiment" which was conducted in the Atlantic Ocean east of Delaware Bay. In the Gulf Stream Experiment, ESTAR mapped a warm core eddy that had broken away from the Gulf Stream while ships provided surface truth. Figure 7 is an example showing the salinity retrieved from ESTAR measurements over a line monitored by the ship, the R/V *Cape Henlopen*. Examples like this helped solidify the case for remote sensing of sea surface salinity from space.

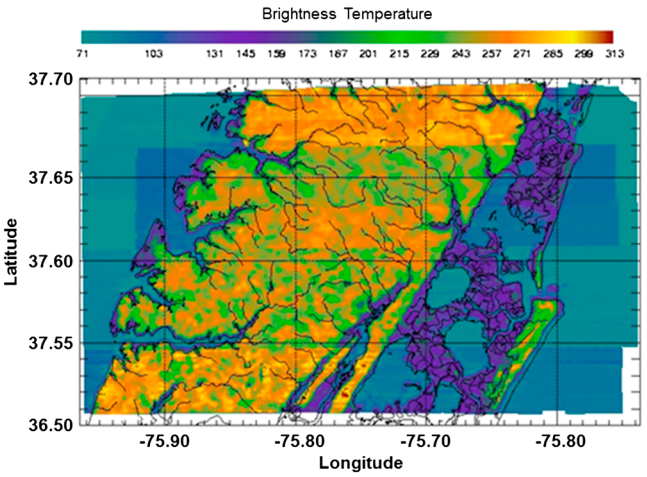

Figure 6. Composite of ESTAR images made during instrument testing [*Swift et al.*, 1991]. The Chesapeake Bay is to the left, and the Atlantic Ocean is to the right. The dark cool area is tidal marsh.

2.3. 2D-STAR

ESTAR has been supplanted by a next generation synthetic aperture radiometer called 2D-STAR designed to demonstrate

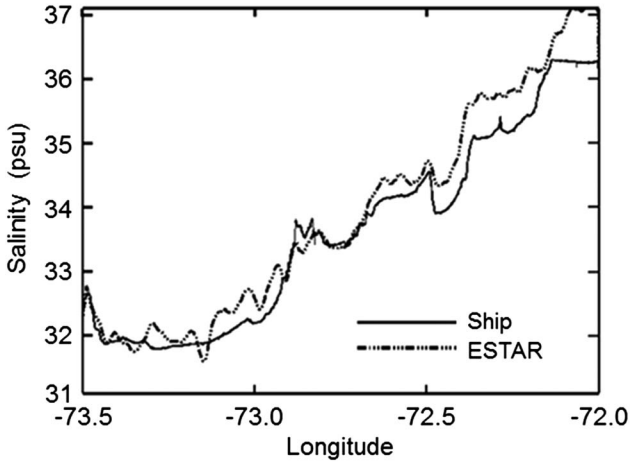

Figure 7. Results from the Gulf Stream Experiment (1999) showing salinity retrieved from ESTAR measurements (broken line) and from a thermosalinograph aboard the R/V *Cape Henlopen*.

the potential for remote sensing applications of aperture synthesis in two dimensions. 2D-STAR was developed under NASA's Instrument Incubator Program as a partnership between the Goddard Space Flight Center, the University of Massachusetts (antenna design), and Prosensing (RF and digital processing and building the hardware). The instrument was first tested in 2002 in the same region of the Delmarva Peninsula used for ESTAR (e.g., Figure 6). In the summer of 2003 it participated in the SMEX03 soil moisture field campaign flying research sites in Alabama, Georgia, and Oklahoma [*Jackson et al.*, 1999], and in the summer of 2004 it participated in SMEX04 flying over sites in Arizona and Mexico.

2D-STAR uses a fully populated, square array of dual polarized patch antennas. Figure 8 (top) is a photograph of the RF box with the radome (the white structure on the left) removed to show the elements of the antenna array. Each patch is square and about 6.86 cm on a side. The patches are dual polarized and separated by 0.5 wavelengths (10.6 cm at L band). The two polarizations are aligned with the principal axes of the array, and in

Figure 8. 2D-STAR antenna and RF box. (top) Earth-viewing side with antenna radome removed. (bottom) Reverse side with cover exposed to show RF receiver hardware arranged in cross configuration.

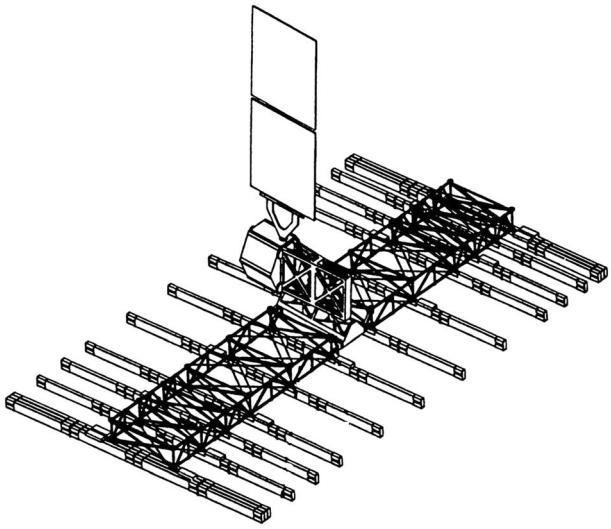

Figure 9. HYDROSTAR in its deployed configuration [*Le Vine*, 1983]. The antenna array is composed of 16 slotted waveguide "stick" antennas.

normal operation one axis is aligned along track (i.e., *X*-pol) and the other across track (*Y*-pol). Although the array is fully populated, only those elements along the principle axes have been used in the synthesis (i.e., a "cross" configuration). Behind each active antenna element is an analog receiver which amplifies and filters the antenna signal and mixes it to IF. Figure 8 (bottom) shows the array from behind where the populated cross is evident. In normal operation, the receiver switches between the two polarizations, but the switching is controlled by a microprocessor, and 2D-STAR can also operate in a single-polarization mode. The receivers are fed a common local oscillator signal and also a correlated noise signal which is used for calibration. The IF signals are digitized, and the complex correlations from all antenna pairs are formed digitally. Each channel can also be connected to an uncorrelated source of noise (terminated load). Additional details of the instrument and design of the correlator can be found in *Le Vine et al*. [2007a, 2007b].

2.4. HYDROSTAR

ESTAR was a "pathfinder" designed to demonstrate the technology of aperture synthesis for eventual application in space. As ESTAR demonstrated success, proposals were made for an instrument in space. The most mature was an ESTAR-like instrument called HYDROSTAR employing aperture synthesis in the cross-track dimension [*Le Vine*, 1999].

HYDROSTAR employed 16 antennas arranged in a minimum redundancy array (Figure 9). The minimum spacing is one-half wavelength, and the antenna array has 90 independent baselines at integer multiples of one-half wavelength. The array spans 9.5 m in the across-track dimension. Each antenna in the array is a rectangular waveguide stick 5.8 m long. The waveguide has 36 slots inclined to produce horizontal polarization and cut in the narrow wall of the guide. Each stick has an along-track beam width of 2.3° at band center corresponding to a resolution of 27 km at nadir from the proposed 670 km orbit. Because waveguides are narrowband devices, operation over the desired bandwidth is obtained by subdividing each stick into four resonant subarrays of nine slots, each coupled together with a flexible combining network. The antennas were to be fabricated in composite to minimize weight and maximize rigidity and thermal stability. The resolution across track matched the along-track resolution at the swath edge (±35°), and at nadir the across-track resolution of the synthesized beam has a peak-to-null beam width of 1.2° corresponding to 14 km resolution. (See *Le Vine* [1999] and *Skou and Le Vine* [2006] for additional details.) Unfortunately, HYDROSTAR was never built.

Research at GSFC has become focused more on SMOS and Aquarius [*Le Vine et al*., 2007a, 2007b, 2010]. But 2D-STAR and ESTAR are still functional, and ESTAR recently participated in a passive/active technology experiment to evaluate a digital beam-forming radar with an across-track footprint similar to that of ESTAR.

3. Interferometry at CNES

3.1. How it All Started

Back in the early 1980s the need for accurate soil moisture measurements became obvious [*Schmugge et al*., 1980], a conclusion further studied and validated during experiments carried out in Western Africa from 1983 to 1992. For instance LERTS-CNES (Laboratoire d'Etudes et de Recherches en Télédétection Spatiale–Centre National d'Etudes Spatiales) studied with INRA (Institut National de la Recherche Agronomique) and CIRAD (Centre International de Recherche en Agronomie et Développement) how to asses the water budget in

Figure 10. Participants to the TUD Interferometry Workshop (from left to right): Christopher Ruf, Helmut Suess, Ulrich Kraft, David Le Vine, Niels Skou, Carmen Capitani, Alberto Resti, Steen Kristensen, Andrew Milman, Jean-Marc Goutoule, Yann Kerr, Alan Thornbury, D. Maccoll, Jay Pearlman, Calvin Swift, and Preben Gudmansen.

aridareas [*Assad et al*., 1986; *Kerr et al*., 1987] for improved crop yield estimates and improved water management and was asked to provide soil moisture information in arid zones for various applications ranging from locust mitigation to weather forecast (e.g., for optimization of sowing dates). These requests led to an extensive search for a means of estimating soil moisture at regional scales and, hence, techniques that could provide soil moisture information from space. As, at that time, no low-frequency radiometer (L band) were available, it seemed useful to evaluate in parallel other potential means to estimate soil moisture and to research ways to have an L band radiometer in space.

The goal of a measurement of soil moisture eliminated use of short wavelengths, but some work was devoted to analyze the potential of thermal infrared. Several approaches were tested but to no avail. The forcings, such as solar radiation and wind speed, by changing the evapotranspiration rate, play a dominant role, making actual soil moisture retrieval intractable as described in a review paper by *Kerr* [2007], either using direct measurements or using thermal inertia. Another alternative was to investigate other wavelengths and everything pointed toward active microwaves with the availability of scatterometer data (ERS-1 SCAT). Actually, radars and SARs (synthetic aperture radars) are usually characterized by low revisit time (typically 10 to 40 days whereas, for monitoring soil moisture, a 3 day revisit is often considered the longest acceptable) but compensated by a high spatial resolution. Another limitation of radar is the difficulty of separating the contribution due to roughness from that of soil moisture which resulted in techniques such as the "change detection approach" [*Moran et al*., 1998, 2002]. All this considered, it confirmed that the use of radar or SAR is inadequate for many areas of the world, in particular, arid and semiarid zones where the "memory" of rain in surface soil moisture is the shortest (both evaporation and percolation rates are high) and the surface roughness (plowing) and vegetation cycle are intimately related to soil moisture variations. Another approach is to use scatterometers which are characterized by a lower spatial resolution and a much higher temporal revisit, adequate for water budget monitoring. The ERS-1 scatterometer offered such an opportunity [*Magagi and Kerr*, 1997a, 1997b, 2001]. It was not adequate for absolute estimates but usable with a change detection approach [*Wagner et al*., 2007]. As a consequence, it was concluded that such approaches are not fully adequate, not delivering absolute values but provided interesting information.

It thus justified investigating further passive microwaves at low frequencies as the ultimate approach to infer soil moisture from space. This led us to seek for a collaboration with US teams and capitalize from the large expertise [*Blanchard et al*., 1981; *Eagleman and Lin*, 1976; *Njoku and Kong*, 1977; *Schmugge et al*., 1974, 1980; *Schmugge and Choudhury*, 1981]. For this we spent some time at Jet Propulsion Laboratory (JPL) working in close collaboration with E. Njoku which led to establishing a radiative transfer model including all components of the signal (soil, vegetation, atmosphere, instrument, and orbit characteristics [*Kerr and Njoku*, 1990]). From then on it was obvious that the only way to infer soil moisture globally and quantitatively was by

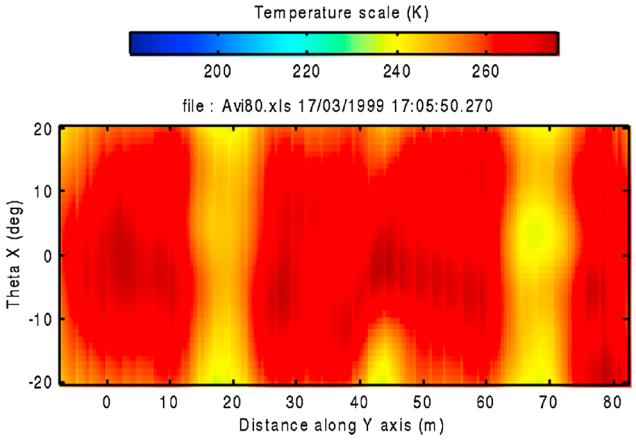

Figure 11. First 2-D interferometry image made over as set of fields in Avignon (1999). From left to right: rough surface, smooth, rough with small water body at top, smooth and rough (refer to *Bayle et al.* [2002]).

using a low-frequency microwave radiometer at L band—in the protected window—as the most appropriate. This simply because it is the only window free of human-made emissions at a frequency low enough to enable soil moisture retrievals while Faraday rotation is still tractable [*Kerr*, 1996; *Kerr et al.*, 2007].

3.2. The Long Path From Concept to Mission

However, once the "optimal" frequency was found, the problem was far from solved. For any microwave sensor, the 3 dB beam width is linked to the wavelength and the antenna aperture. At L band (21 cm) with a Sun-synchronous orbit and an appropriate temporal revisit (e.g., orbit altitudes of 650–750 km) and spatial resolution (e.g., 50 km), the result is an antenna size of around 8 m which looked very daunting. Several paths to achieve this challenge have been investigated since. A very novel approach developed in the US and which led to the ESTAR concept [*Le Vine et al.*, 1994, 1989, 1990] was used at LERTS as a starting point. We opted very early to follow this idea. It was initiated through a joint CNES–Matra Marconi Space (MMS) funded thesis at LERTS, which was initiated in 1988 [*Thibaut*, 1994] on the imaging concept as well as one more oriented toward signal processing [*Anterrieu*, 1992]. During the first study, through Thibaud's thesis work [*Thibaut*, 1994], we developed a very simple interferometer simulator and ran it on a simulated L band scene made from an advanced very high resolution radiometer scene [*Thibaut and Kerr*, 1990; *Thibaut et al.*, 1990]. We were very quickly convinced of the potential of this approach. However, the approach solved only half of the problem as we only had a reduced antenna dimension in one direction. Discussions with radio astronomers (André Lannes and his team) of the Observatoire du Pic du Midi, Toulouse (OMP), led us very quickly to consider 2-D interferometry as used in some very long baseline interferometry and very large array approaches. In 1991 André Lannes proposed the first concept with J. M. Goutoule from MMS and Y. Kerr from LERTS. It was based upon a Y-shaped interferometer. The subsequent years were devoted to both improving the concept as well as refining the science objectives.

In 1991 an international workshop [*Skou*, 1991] was organized at DTU to investigate all possible designs with a significant push toward 2-D interferometer designs (Figure 10). It was linked to the fact that ESA became interested in the venture and actually initiated the so-called MIRAS (Microwave Imaging Radiometer using Aperture Synthesis) Project. This project involved the same three groups in Toulouse from MMS, OMP, and LERTS and was funded by ESA (MIRAS study [*Goutoule et al.*, 1996]). This study demonstrated that the Y-shaped approach was the optimum in terms of frequency coverage, sensitivity, and implementation as demonstrated previously by radio astronomers. So all subsequent studies made in the framework of MIRAS-SMOS were based upon this approach. In the very early years, the concept was only considered as having the potential for delivering a pseudo conical scan. It was only through a comment by Dr. T. J. Schmugge that the full potential became obvious (getting the entire angular signature rather than a simple conical scan).

Work was carried out on several fronts. Obviously, at MMS they looked at the practical concept including making an 11-element airborne demonstrator (MIRAS-11 demonstrator [*Bayle et al.*, 2002]; see Figure 20 and section 6.3 below) as well as the instrument design for a potential space mission (the MIRAS project, section 6.2 below). LERTS considered the potential use of SMOS, both over land and linking the gap with oceanographers, making field campaigns and developing intense modeling activities (with INRA) including airborne campaigns with the Portos instrument (mainly 1991–1992) and ground-based intensive campaigns using the ground version of PORTOS (which had the L band frequency) mainly in 1990, 1991, and 1993. PORTOS is a multifrequency dual polarized microwave radiometer which was used with two configurations either airborne with frequencies ranging from 6.7 to 90 GHz (as for AMSR) [*Chanzy et al.*, 1997] or at ground

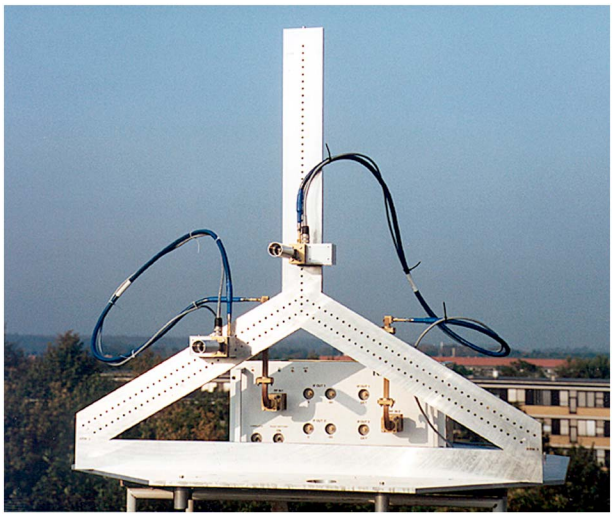

Figure 12. Far-field setup intended to simulate the SMOS concept.

level with the added 1.4 GHz channel [*Wigneron et al*., 1993; *Raju et al*., 1995]. The data are still being used today [*Tsang et al*., 2013]. These activities led to the consolidation of the Earth Vegetation Atmosphere model [*Kerr and Njoku*, 1990] into the L band Model of the Emission of the Biosphere [*Wigneron et al*., 2007]. In parallel, at OMP and then at the Centre d'Etudes et de Recherches (CERFACS), the interferometric concept was further refined and modeled with several thesis and modeling activities led by Prof. A. Lannes.

Using the results mentioned above, and in parallel to the MIRAS project, several proposals were submitted to various agencies to have an L band 2-D interferometer in space. It can only be said that all were turned down. It is worth mentioning that a SMOS-like concept was also proposed—but at X band—to infer rainfall over the ocean in a Tropical Rainfall Measuring Mission-like mission.

When the concept was mature enough and the MIRAS project was in full swing, France decided to withdraw from the ESA program through which MIRAS was to be financed (GSTP (General Support Technology Program) program), making its future somewhat doomed as France was the main source of funding. Several attempts were made by the scientific community and the industry in France to convince the decision makers to alter their decision, but to no avail. Luckily, ESA managed to convince other countries, among them Spain, to pick up the slack, putting the MIRAS study back on track. EADS-CASA (European Aeronautic Defence and Space-Construcciones Aeronáuticas Sociedad Anónima) Espacio, MIER Comunicaciones, and the Polytechnic University of Catalonia (UPC), among other European companies and universities, continued the work started by MMS and OMP/CERFACS, saving the concept. At about the same time LERTS became CESBIO (Centre d'Etudes Spatiales de la Biosphère) and was able to keep on working on the concept, being purely scientific and not requiring ESA's GSTP funding.

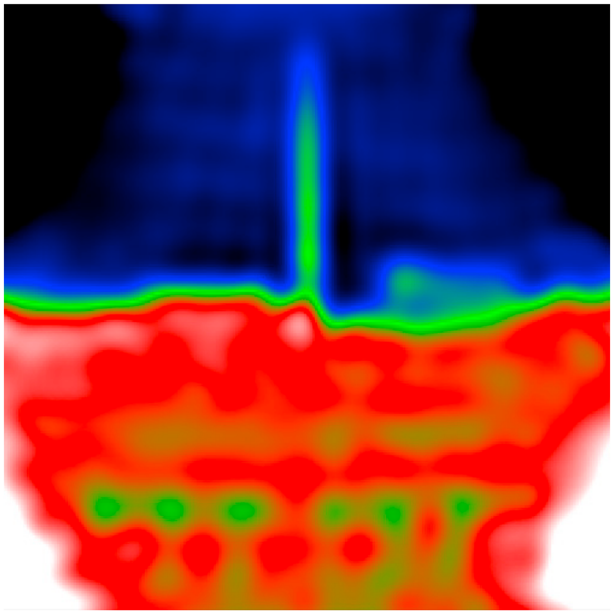

Figure 13. Skyline at DTU imaged by the far-field system.

CNES was, however, still active and was working on several aspects of the 2-D interferometry including an airborne demonstrator. For this they took a new approach (O. Grosjean), transforming the concept into an equilateral triangle to reduce volume and making it easier to fit on board the French research aircraft. The concept proved to have several advantages including ease of implementation while retaining the advantages of the Y-shaped concept which made it implementable on the French research aircraft (ATR 42). There again the project was out of luck as CNES decided to stop all airborne activities. As a result, this concept never left the drawing board. So, to summarize those early years, in 1996, the concept was already 7 years old, an

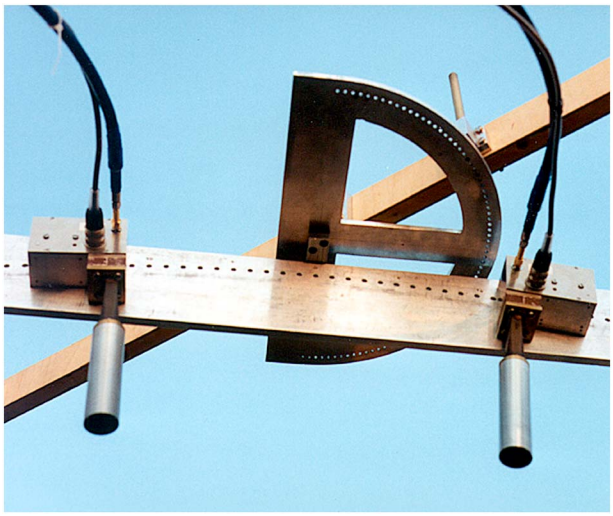

Figure 14. Focused, near-field setup.

ESA demonstrator built by MMS had been made (but only tested in flight, never used), and a demonstrator designed at CNES was never made.

Nevertheless, the concept had been saved because of the technical activities with other countries and because a spaceborne concept (MIRAS) existed. On the science side, much work had been carried out on modeling and simulation (from Faraday rotation and effect of the atmosphere on propagation to water interception on vegetation) together with several intensive field experiments in Avignon. To achieve a general consensus, several workshops were organized. A large scientific one was held in St. Lary France in 1993 [*Choudhury et al*., 1995] and a Soil Moisture and Ocean Salinity retrieval from space workshop was held at ESTEC in 1995 (Consultative Meeting on "Soil Moisture and Ocean Salinity: Measurement Requirements and Radiometer Techniques," ESA Workshop Proceedings WPP-87, ESTEC, Noordwijk, The Netherlands, 20–21 April 1995). During the first of these workshops, the science requirements for such a mission were laid out [*Kerr et al*., 1995] while the second one was focused more on the 2-D interferometric concept.

After that the concept was consolidated, the first fully developed 2-D interferometric proposal was submitted to the CNES for the "séminaire de prospective scientifique" in 1997 [*Kerr*, 1997]. The proposal was selected with the caveat of finding additional funding. The ESA Earth Explorer Opportunity mission program provided a unique opportunity almost a year later. This time interval was put into good use to finalize a number of elements (selection of the orbit, design of the deployment mechanism, choice of a bus, etc.) and to enhance the team with a larger contribution from Europe and Spain in particular. A new proposal was submitted to ESA in November 1998 [*Kerr*, 1998] and selected. The SMOS instrument and mission were born after almost a decade of effort. It is worth mentioning that most of the features of the 1998 proposal were endorsed during the phase A to C/D development and correspond to the final mission apart from a fine tuning of the observation geometry (antenna spacing, tilt, and steer angle) which was performed during the definition phase [*Waldteufel et al*., 2003].

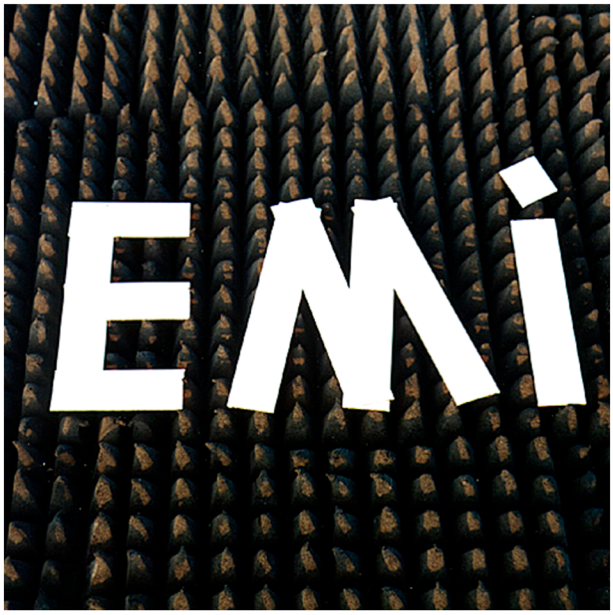

Figure 15. Metal letters to be imaged by the focused system.

Next it was necessary to produce a proof of concept, and for this purpose CESBIO with CNES INRA and Astrium refurbished the MIRAS-11 demonstrator (not completely though as we missed the scene temperature radiometer) and operated it in Avignon, France. The first ever 2-D interferometric image of a land surface was produced by traveling the MIRAS-11 demonstrator over plowed and irrigated fields in Avignon in 1999. The image was poor [*Bayle et al*., 2002] but proved the concept (see Figure 11).

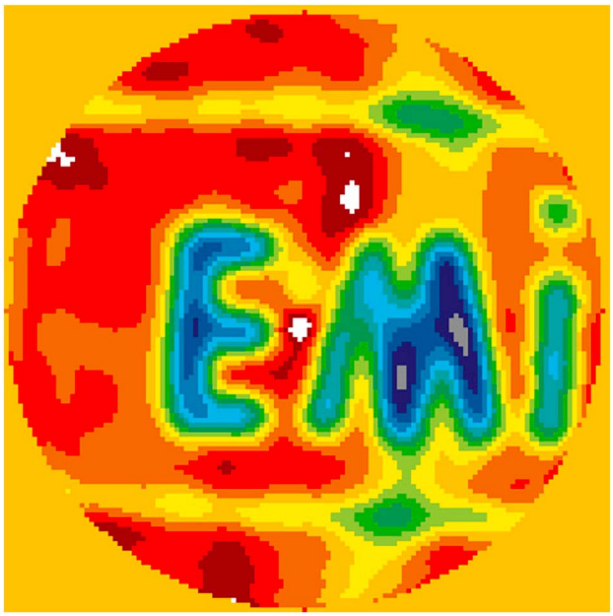

Figure 16. Reconstructed brightness image of the metal letters.

As soon as the project was selected by ESA, work progressed smoothly with contributions from CNES and CDTI. The science activities performed in parallel led to a very successful and important scientific return from the mission very soon after launch (see IEEE special issues on SMOS [*Kerr et al.*, 2012] and over 400 papers published in total on SMOS).

4. Interferometry at DTU

In the early 1990s, research on aperture synthesis started at DTU, and a Synthetic Aperture Radiometer (SARad) demonstration model consisting of a two-channel X band correlation radiometer with two horn antennas and an antenna mounting structure enabling the horns to be mounted in relevant positions within the aperture was developed [*Laursen et al.* 1995]. This was soon superseded by an improved Ku-band system [*Laursen and Skou*, 1998]. A complete aperture synthesis is obtained by sequentially placing the two antenna elements in all required pair combinations and measuring the corresponding samples of the visibility function. These two systems were used to demonstrate two-dimensional synthetic aperture imaging of complex targets in outdoor ground experiments.

Systems such as these, which require a single pair of antennas to be moved sequentially to different positions, require the test scene to remain stable during the measurements, typically a few hours. They can be used to demonstrate the synthetic aperture concept in ground-based experiments, but they cannot be used as remote sensors when the scene (or platform) is not stationary.

Figure 12 shows the Ku-band system in a far-field setup intended to simulate the SMOS concept with its typical Y-shaped antenna structure. The antennas are small circular dual mode horns with a 1.5λ diameter, and they are connected with the correlation radiometer by phase stable cables. Among the challenges is that a large distance to the target is required to get into the far field of the synthesized antenna. Thus, a "normal" ground setup with the instrument looking down from a tower is not practical. Figures 12 and 13 shows a horizontal setup where the "skyline" as seen from a roof at DTU is imaged. One clearly sees the border between buildings and the sky, with a large power plant chimney being imaged. The fundamental imaging concept is demonstrated, although not very satisfactorily due to the simple target.

In Figure 14 the same antenna elements are used in a near-field setup, and now the elements are mounted on a curved rail. By using different positions on the rail, and by rotating this rail around a vertical axis, the full aperture is covered. The curved rail implies that the system has a focused antenna system, thus enabling a short distance to the target. Provided that the elements are placed symmetrically about the rotation axis, image reconstruction algorithms identical to those used in a normal far-field situation can be utilized. The sampling distance (or the minimum antenna spacing) is 1.57λ, and all visibility samples are measured. The maximum aperture is 32λ, resulting in a synthetic beam width of 2.2° at nadir and an image size of 18×18 pixels. The reconstruction algorithm can be based on a fast Fourier transform (FFT) only when there is no coupling between the antennas. The coupling between the dual mode circular horns was measured to be −45 dB (worst case) and can be ignored. The rotation of the rail, and associated rotation of the antenna elements, also means a requirement for an unpolarized target and identical radiation patterns in E and H planes within the ±19° used for imaging. The antenna patterns had rotation symmetry to within 0.12 dB, but even this may result in errors of up to 4.2 K in the final image.

The two-channel correlation radiometer operates at 16.25 GHz and the system bandwidth is 100 MHz. Analog correlators in the form of four quadrant multipliers followed by integrators were used in the system, and phase switching was used to reduce correlator offsets.

The target in Figure 15 consists of three metal letters spelling "EMI" placed on top of microwave absorbers. The measurements were taken outdoors, so the metal letters reflect the cold sky temperature. The letters were made out of metal sticks with a width of 5 cm, which matches the theoretical resolution at the center of the image using a Hamming weighting function.

Figure 16 shows the image after proper reconstruction. It is evident that the letters EMI are imaged with a cold signature (bluish) on a generally warm (reddish) background. Many disturbances are also seen. These are due to issues such as nonperfect instrument stability, calibration errors, correlator offsets, and antenna patterns asymmetries. In addition, in this case the imperfect setup also contributed (the antenna system and the cables to the radiometer, as well as the wooden structure that carries the antenna, are all in the field of view when the cold sky is reflected by the letters). Furthermore, the structure may also be aliased into the image and cause errors.

Nevertheless, using simple hardware (only two radiometer channels) it was possible to demonstrate the concept of aperture synthesis in two dimensions and also experience some of the problems associated with this technique.

5. Aperture Synthesis Imaging at DLR

5.1. Motivation

In addition to Earth observation and military applications, microwave radiometry has been considered as a tool for security and safety imaging applications [*Grüner et al*., 1992; *Peichl et al*. 2007], (Various authors, Proc. of SPIE, Defence, Security and Sensing, Passive Millimetre-Wave Technology, Vol. I to Vol. XVI, 1998–2013), (Assessment of MMW and Terahertz Technology for Detection and Identification of Concealed Explosives and Weapons, Committee on Assessment of Security Technologies for Transportation, National Materials Advisory Board, Division on Engineering and Physical Sciences, National Research Council on the National Academies, The National Academies Press, Washington, D.C., USA, www.nap.edu, 2007). A major reason for this is that the technology has become mature enough to construct reliable sensors at moderate costs. High-performance passive microwave and millimeter-wave imaging can provide improved situational awareness due to its capability to produce quasi-optical images in adverse viewing conditions (e.g., rain, fog, dust, smoke) during day and night time, and to penetrate many dielectric materials allowing the detection of concealed objects (e.g., weapons under clothing, buried landmines, and through-wall imaging). However, the technological requirements are challenging given the requirements for real-time imaging capability, large field of view, high spatial resolution, and high sensitivity. Aperture synthesis has been investigated at the DLR, Microwaves and Radar Institute, as a candidate for such high-performance passive imaging, keeping in mind the goal of reasonable expense and budget.

5.2. Proof of Principle Demonstrator ASR (Aperture Synthesis Radiometer)

In 1990 DLR started theoretical analysis and experimental validation of the feasibility of the aperture synthesis principle for Earth observation applications. A two-element-interferometer was constructed using analog correlation techniques at 37 GHz and in a "T" configuration with variable baselines as shown in Figure 17 (left). In Figure 17 (right) is shown a high-resolution image together with a photograph of the scene, which demonstrated the feasibility of aperture synthesis for Earth observation applications even in the millimeter-wave domain [*Peichl et al*., 1998]. The individual targets can be recognized clearly by shape and size. Another very important finding around 1995 was that by aperture synthesis adaptive focusing in the very near field or the far field is possible just by mathematical means without changing the hardware. DLR continued activities on aperture synthesis in 1999 by participating as a scientific consultant in the SMOS Science Advisory Group and continued until 2010 when the SMOS satellite was launched and the group was disbanded (replaced by the Quality Working Group). Within that period various studies on problems related to SMOS have been carried out [*Peichl et al*., 2000; *Greiner et al*., 2003; *Peichl and Süß*, 2005; *Peichl et al*., 2005].

5.3. Microwave Imaging Spectrometer ANSAS

In order to obtain information on a scene and permitting imaging of hidden structures like buried landmines [*Peichl et al.*, 1996, *Peichl et al*., 2001], a spectral analysis in the lower microwave region is suitable. Such

Figure 17. (left) Photograph of the two-element interferometer ASR with variable baselines for investigating the principle of aperture synthesis. (middle) Photograph of a test scene. (right) Reconstructed Ka band image of the test scene applying near-field focusing, angular resolution is about 0.4°, distance to targets is between 15 m and 30 m.

requirements can be addressed by using broadband multichannel aperture synthesis techniques. The experience from landmine detection research using microwave radiometers and from aperture synthesis research, both led to the development of a new imaging concept in the middle 2000s. ANSAS (Abbildendes Niederfrequenz-Spektrometer mit AperturSynthese), shown in Figure 18 (left), is a one-dimensional aperture synthesis array operating in the frequency range of about 1.4–6.5 GHz, where narrowband sampling (e.g., 20 MHz) at any arbitrary center frequency is possible [*Jirousek et al*., 2010]. For the second image dimension a rotation of the linear array is performed, leading to a hybrid instrument combining a mechanical motion and electronic beam steering by aperture synthesis. The array is up to 3 m in length and has 15 receivers and 105 correlators, the latter being implemented in one-bit digital technology on a Field Programmable Gate Array.

The single antennas are of broadband Vivaldi type on microstrip technology, allowing a close distance for the minimum baseline. The images show clearly the Earth and sky region and several targets like a metal plate and different ground texture, although major error sources have not been removed yet.

5.4. Proof of Principle Demonstrator VESAS

Research in the early and middle 2000s on high-performance passive millimeter-wave imaging for security applications led to the investigation of sensor concepts with high frame rates at moderate expense and costs [*Peichl et al*., 2007]. A concept for novel low-cost fully electronic scanning was investigated at Ka band by VESAS (VollElektronsicher Scanner mit AperturSynthese) [*Schreiber et al*., 2010]. Two-dimensional scanning is realized by frequency scanning in one direction (i.e., beam steering by changing the received frequency band between 31 GHz and 39 GHz) and using aperture synthesis in the other direction, as illustrated in Figure 19 (left). The design goals, in this case, were to achieve an image frame rate of around 1 s, a spatial resolution of about 0.4° in both dimensions and a field of view of around 25° × 60°. The frequency-dependent beam steering capability of a slotted waveguide antenna provides an image line. Spatial frequency sampling in the orthogonal

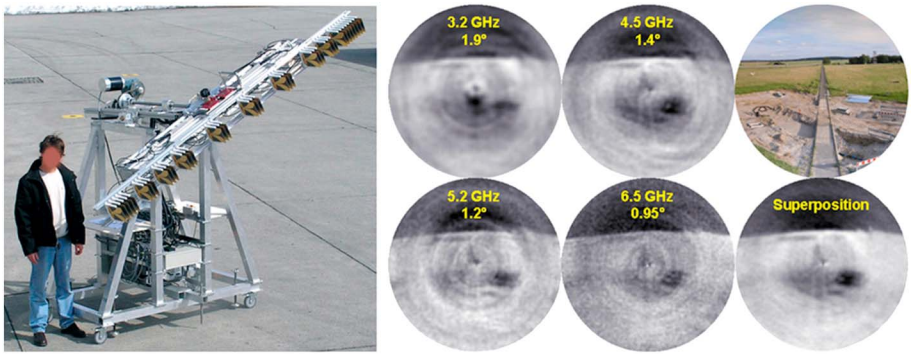

Figure 18. (left) Photograph of the ANSAS system. (right) Photograph of a test scene and corresponding reconstructed images for various frequencies (angular resolutions) and a superposition of the single images; up to now antenna patterns and mutual coupling are not fully corrected for. Field of view diameter is roughly 80°–100°.

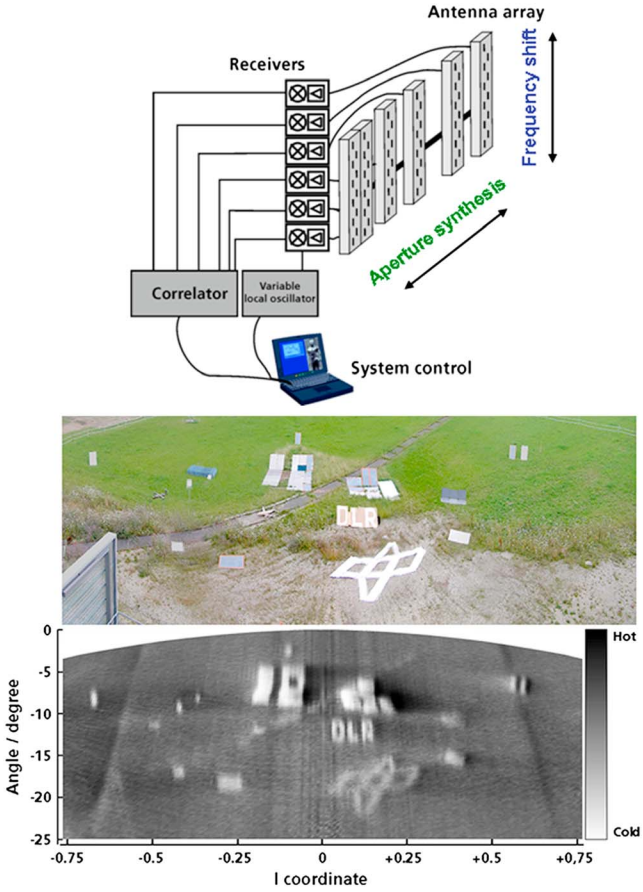

Figure 19. (left) Sketch of the VESAS imaging principle. (right) Photograph and reconstructed Ka band image of a test scene containing various metallic and nonmetallic objects. Note that the shown width of the image scaled as directional cosine $l = \sin\Theta$ is about 100°. Angular resolution is 1° for a 0.5 m antenna length. Distance to targets is between 20 and 50 m.

direction is achieved by a low redundancy, thinned array of such antennas. For a proof of concept, an experimental system based on a two-element interferometer was used. The required signal correlation is performed either in analog or digital techniques. Typically, a bandwidth of 100 MHz is used per frequency sample. Depending on the steps of the frequency scan, the image acquisition time for the interferometer is in the order of a few 10 min. The example image shown clearly demonstrates the feasibility of this imaging method. It is estimated that the final array for an aperture size of 1.3 m × 1.3 m and a corresponding angular resolution of 0.4° would require only around 35 receivers.

6. Development of MIRAS at the European Space Agency

6.1. Historical Review

Following the successful development of ESTAR at the NASA Goddard Space Flight Center and the University of Massachusetts, Amherst during the 1980s (see section 2), in May 1991 ESA organized a workshop on "Advanced Microwave Radiometer Techniques," hosted by the Technical University of Denmark (DTU) in Copenhagen [*Skou*, 1991]. Leading experts from the microwave communities in Europe and the USA discussed conical scan, push broom, and interferometric techniques in an attempt to identify new avenues of research. One of the recommendations from this workshop was the study of a two-dimensional aperture synthesis radiometer and its calibration system, which were little understood at that time. The first step was the building of a laboratory demonstration model, and this was successfully undertaken by DTU at X band (described in section 4).

In view of the recommendations of the Copenhagen Workshop and the encouraging results of ESTAR and the DTU demonstrator, in 1993 ESA initiated the MIRAS feasibility study as a "Microwave Radiometry Critical Technology Development" ("Microwave Radiometry Critical Technical Development," Statement of Work, ESTEC XRI/177.92, September 1992). The scientific goals for MIRAS were established by CESBIO (refer to section 2). In April 1995, ESA organized "SMOS," a "Consultative Meeting on Soil Moisture and Ocean Salinity Measurement Requirements and Radiometer Techniques," which brought together both the international scientific community and representatives of industry (Consultative Meeting on "Soil Moisture and Ocean Salinity: Measurement Requirements and Radiometer Techniques," ESA Workshop Proceedings WPP-87, ESTEC, Noordwijk, The Netherlands, 20–21 April 1995). This dialog reconfirmed the need for and importance of mapping soil moisture and ocean salinity from space.

By the end of 1996, the MIRAS feasibility study had been completed and both the first theoretical analysis of a spaceborne instrument and the development of an aircraft prototype had been performed [*Martín-Neira and Goutoule*, 1997]. Additional studies were launched in parallel between 1994 and 1996 to study specific topics such as calibration techniques, dual polarization capability, the bidimensional discrete formulation of aperture

synthesis, a dual-frequency L + C band MIRAS instrument and an in-orbit demonstrator to fly one MIRAS arm on the Spanish MiniSat platform. The critical technologies had also been identified, and between 1995 and 1998 the first prototypes of LICEF-1 (Light Weight Cost Effective Antenna Front-end Assembly) receivers and DICOS-1 (Advanced Digital Correlator Unit for Aperture Synthesis Application) correlator were built.

ESA and NASA held several technical interchange meetings on L/C band aperture synthesis where progress on MIRAS and HYDROSTAR (described later) was reported (June 1996 and July 1998 at GSFC, April 1999 at Irvine, CA). CNES joined the second one where a white paper on Aperture Synthesis Technology Road Map for Observation of Soil Moisture and Ocean Salinity was written [*Engman et al*., 1998].

In 1998 ESA started the MIRAS Demonstrator Pilot Project (MDPP) as a major attempt to provide a technology solution to the problem of L band aperture synthesis radiometry [*Martín-Neira et al*., 2002]. The objectives were to build a representative part of MIRAS with technologies suitable for space and to arrange this hardware in the form of an airborne demonstrator for end-to-end concept demonstration. This included the production of the second generation of receivers (12 LICEF-2 units) and correlator (DICOS-2) with ASICs (Application Specific Integrated Circuit) suited for space application. It also included a first generation of the Noise Injection Radiometer (NIR-1), the onboard Calibration System (CAS-1), the MIRAS Optical Harness (MOHA-1), the Control and Monitoring Note (CMN-1) units as well as of the deployment mechanisms and the arm structure, including a first full-arm deployment demonstration.

The MDPP went into three main phases, MDPP-1 through MDPP-3, kicked off in 1998, 2001, and 2004, respectively. The first image validation test with the complete MDPP hardware inside an electromagnetic compatibility chamber took place in November 2002, the outcome of which led to a new formulation of the fundamental equation of aperture synthesis radiometry, the Corbella equation [*Corbella et al*., 2004]. This new equation represented a significant step toward understanding the image validation test observations which did not fit the theory used in radio astronomy. In parallel with the MDPP Pilot Project, several field image validation tests were conducted using a few LICEF receivers and a dedicated DICOS-3 correlator, whose main objective was the verification of the new equation using the cold sky.

The onboard calibration system implemented in the MDPP hardware was based on the studies conducted at the Polytechnic University of Catalonia (UPC) and the concurrent experience of the Finnish Helsinki University of Technology (HUT)-2D interferometer development by the Helsinki University of Technology (section 8 below). With its maiden flight in May 2006, HUT-2D became the first airborne two-dimensional L band aperture synthesis radiometer providing high-quality images based on the Corbella equation and its associated flat target transformation (FTT) calibration technique [*Martín-Neira et al*., 2008]. Shortly after, in June 2006, the first flight of the MDPP Airborne MIRAS demonstrator (AMIRAS) took place with similar results. HUT-2D and AMIRAS were two key milestones in the overall development and demonstration of the SMOS mission before its launch.

In the meantime 13 July 1998 ESA issued a Call for Proposals for Earth Explorer Opportunity Missions with a deadline for receipt of proposals 1 December 1998. Twenty seven proposals were received, one of them the SMOS proposal, submitted by CESBIO together with Institut de Ciències del Mar (ICM), CNES, and CDTI [*Kerr*, 1998]. On 27 April 1999, ESA's Earth Science Advisory Committee recommended the implementation of the SMOS mission as second Earth Explorer Opportunity Mission (following (CRYOSAT) Cryosphere and SAT for Satellite). This recommendation was later confirmed by the Program Board for Earth Observation on 18 May 1999.

The SMOS Project Phase A started 13 September 2000 and lasted until 17 December 2001. An extension of Phase A ran from 2 February 2002 till 28 November 2002, which was followed by Phase B, from 28 November 2002 until 10 December 2003. The Corbella equation was developed during this phase of the SMOS project within the parallel MIRAS Demonstrator Pilot Project. The Phase C/D of SMOS started 10 December 2003 and ended with its launch.

SMOS was launched Monday 2 November 2009 at 02:50:51 from the cosmodrome of Pletsetsk, in Northern Russia. The next day the antenna of MIRAS was opened, and the instrument was switched on 17 November 2009, at which time the first signal acquisition from ESAC ground station also happened. Two days later, 19 November 2009, the first worldwide brightness temperature image from SMOS was produced. The same day, the first soil moisture retrieval image was generated along the West Coast of North America. The first calibrated sky image, including the Milky Way and the Moon, came on 20 January 2010, and the first map of sea surface salinity, of the Pacific Ocean, was released 10 February 2010.

Figure 20. MIRAS Airborne Demonstrator (Matra Marconi Space, 1996).

From the very beginning it was clear emissions of significant strength in the 1400–1427 MHz protected band were a problem. The spatial resolution of SMOS allows locating these RFI sources and, with the collaboration of national frequency coordination offices, many have been turned off. The first RFI that was turned off (15 March 2010) was a television radio link in the peak of Villuercas (Spain) that was affecting SMOS images 3000 km away. Since then over 200 RFI sources around the world have been switched off following the same procedure.

The commissioning phase of SMOS took about 6 months until it was declared operational 20 May 2010. A few anomalies have occurred on board, but none of them serious enough so as to impact the quality of the data. The two most important ones were the unlocking of the local oscillator of segment A2 which would not relock onto the proper frequency (December 2009) and the wrong temperature readings in segment B1 (Dec 2010) which affected its thermal control. As a result, arms A and B were switched to their redundant sides.

SMOS has already passed the end of its nominal lifetime of 3 years. During this time much has been learned both at the level of calibrating the brightness temperature images as well as in the retrieval methods for soil moisture and ocean salinity. There was no precedent. Hence, everything had to be done basically from scratch, the most difficult part perhaps being the full understanding of the instrument principles and the data processing and calibration of its very wide field of view images. The learning curve is still positive, but already it can be stated that SMOS has fully proven the aperture synthesis technique for remote sensing of the Earth.

6.2. MIRAS on Envisat Study

The first study on MIRAS undertaken by ESA resulted in a spaceborne instrument design of 133 elements distributed over a Y-shaped array with arms 8.3 m long. The elements were spaced 0.89λ, and the entire array was tilted 31.2° forward with respect to nadir and designed to have a 70° field of view [*Martín-Neira*, 1993]. The instrument operated in dual linear polarization (horizontal and vertical). Each antenna was to be connected to a MMIC (Monolithic Microwave Integrated Circuit) L band receiver which amplified and down-converted the H and V signals sequentially. After one-bit digitization, the baseband digital signals would be routed to the correlators via optical fibers, to minimize the effects of gain and phase drifts. The 8778 correlations, which were simply the complex multiplication and integration of any pair of receiver outputs, were to be performed by 1 bit digital correlators implemented in a single correlator unit. The estimated MIRAS weight and power consumption were of 230 kg and 300 W, respectively. It was supposed to fly aboard Envisat.

6.3. First MIRAS Airborne Demonstrator and Avignon Campaign

The first MIRAS breadboard built for ESA (by Matra Marconi Space–MMS) was a scaled-down airborne version of the previous spaceborne instrument (Figure 20). This MIRAS breadboard was a Y-shaped array with arms 0.65 m long, with elements spaced 0.89λ, and with 11 antenna elements, including an additional element to provide phase-restoration capability. The mounting on board the aircraft still allowed an alias-free region around the 50° incidence angle range of interest. Both V and H polarizations were measured alternately and

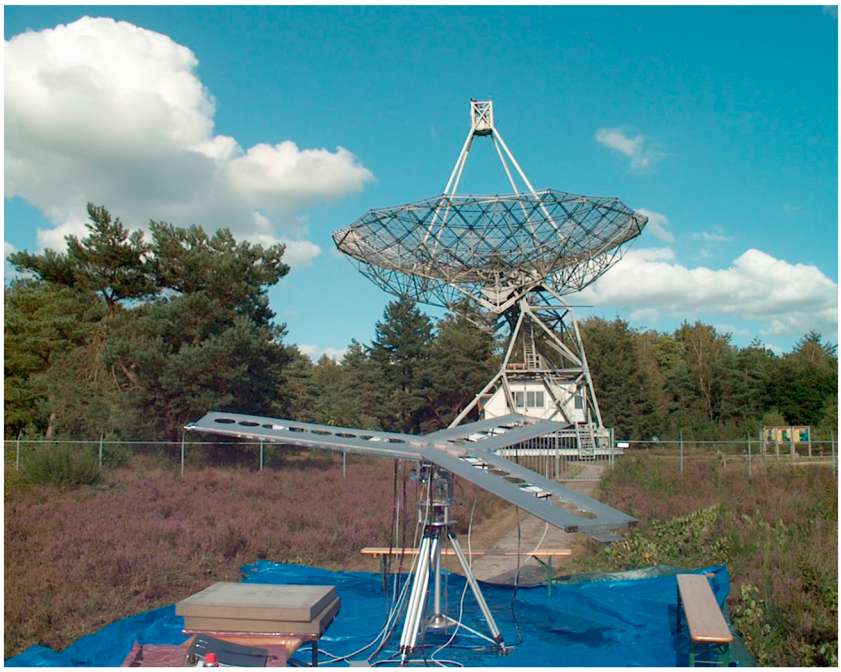

Figure 21. First ESA ground tests at Dwingeloo (equipment from MIER Comunicaciones, Astrium-Ottobrun and YLINEN, 2001–2006).

every 3 or 5 s calibration signals, consisting of either uncorrelated or correlated signals, were injected at the receivers input ports.

MIRAS was flown twice on board a Hercules C-130 in November and December 1997, but technical problems were encountered in both flights. Some visibility measurements seemed to show variations correlated with the coastlines, but no images could be generated. In March 1999, the breadboard was mounted on a crane boom at the Institut National de la Recherche Agronomique by CNES and CESBIO, helped by MMS.

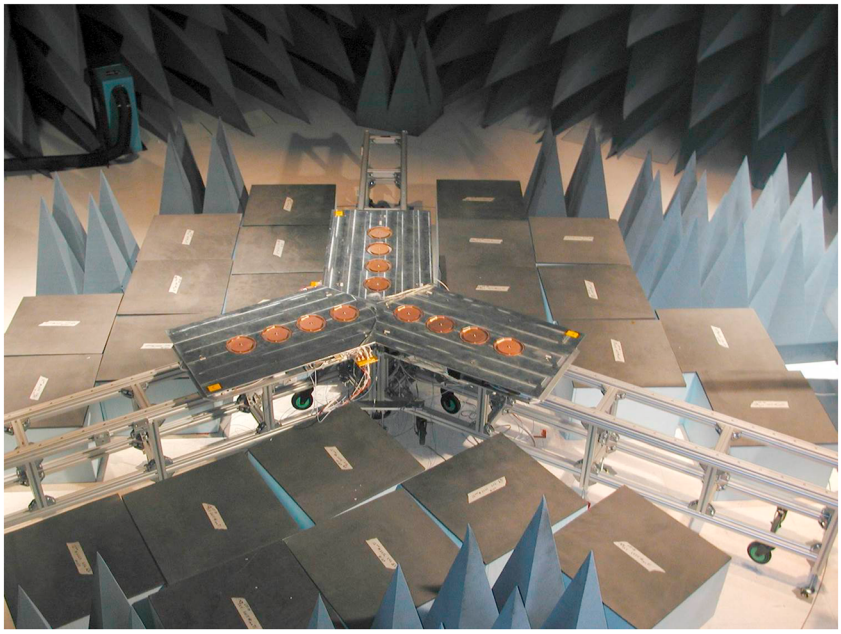

Figure 22. MDPP ground demonstrator (EADS-CASA Espacio, November 2002).

Figure 23. AMIRAS installed in Helsinki University of Tecnology's Short-SC7 Skyvan Aircraft (June 2006).

Observations over different test fields, including a pool of water, were carried out, and the main emissivity patterns of the observed scenes retrieved (Figure 11).

6.4. First Ground Demonstrators

The two LICEF-1 receivers (by MIER Comunicaciones) and the DICOS-3 correlator unit (by Astrium-Ottobrun) described earlier were assembled in a first version of a ground demonstrator to carry out some open door experiments at the Dwingeloo radio observatory (Figure 21). Each arm was six spacings (0.942λ) long. The Sun and the Moon were the targets of three experiments carried out between September 2001 and March 2002. The same hardware was used in imaging tests at the Polytechnic University of Valencia (November 2001) and DLR (August 2004) too.

The NIR-1 (by YLINEN) and three LICEF-2 units together with an upgraded DICOS-3B correlator were later integrated in an improved ground demonstrator with nine spacing (0.89λ) long arms. This enhanced ground demonstrator allowed verifying the Corbella equation inside an electromagnetic compatibility test chamber and outdoors by imaging the cold sky at Dwingeloo in September 2004. Except in the DLR setup, in all other cases the receivers had to be moved manually into all possible positions to acquire all visibilities.

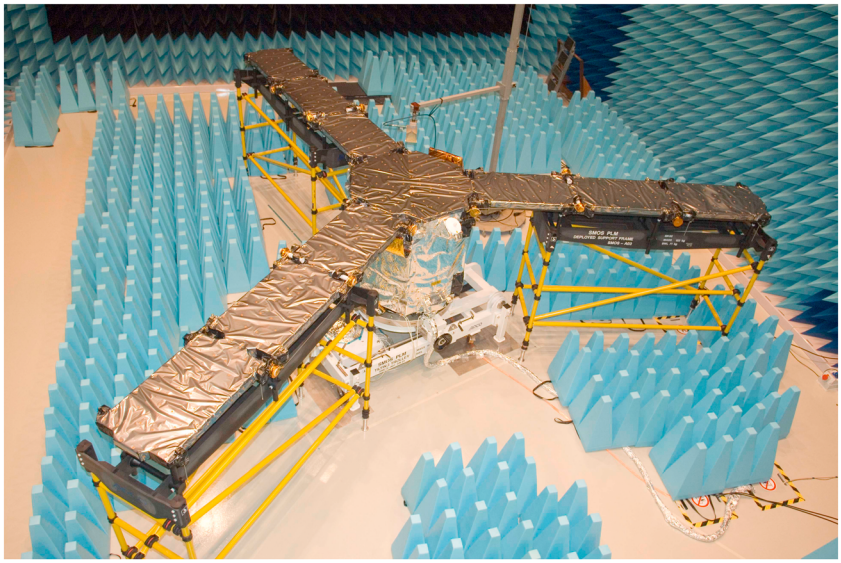

Figure 24. MIRAS in the Maxwell EMC Chamber at ESTEC (May 2007).

6.5. MDPP Ground Demonstrator

The largest and most advanced MIRAS ground demonstrator was built from the electronic units produced from the MIRAS Demonstrator Pilot Project (led by EADS-CASA Espacio). A set of four LICEF-2 receivers was mounted on a carriage which could slide along one arm in three different positions to achieve up to 12 spacings of 0.89λ. The other two arms were built the same way. The optical harness MOHA-1 and the DICOS-1 correlator unit formed part of this breadboard, as well as the onboard calibration system CAS (by Helsinki University of Technology). The first image validation test with this breadboard took place in the INTA (Instituto Nacional de Técnica Aeroespacial) electromagnetic compatibility chamber in November 2002 and led to the formulation of the Corbella equation (Figure 22).

6.6. AMIRAS

The hardware of the MIRAS Demonstrator Pilot Project was finally arranged into an Airborne MIRAS (AMIRAS) demonstrator with the hardware most similar to SMOS ever, for which reason it was also referred to as "SMOSillo" ("small SMOS"). AMIRAS included the NIR-1, all 12 LICEF-2 receivers, the DICOS-2 correlator, the CAS calibration system, and two CMN units, but not the optical harness for complexity reasons, which was replaced by an electrical harness. This SMOSillo had only four elements per arm, with the NIR receiver at the center, all spaced by 0.875λ as SMOS. SMOSillo could work in dual-pol as well as full polarimetric mode. The same ASICs of DICOS-2 used in SMOSillo were the ones later flown on SMOS. AMIRAS successfully imaged Cygnus April 2006 and was first flown in June and July 2006 on the Skyvan aircraft of the Helsinki University of Technology (Figure 23). The high-quality images delivered during these flights (by UPC) significantly helped to verify the SMOS concept [*Corbella et al*., 2008].

6.7. SMOS

ESA's Soil Moisture and Ocean Salinity (SMOS) spaceborne mission was developed in cooperation with CNES and CDTI. It contained a single payload, MIRAS, the first microwave imaging radiometer with two-dimensional aperture synthesis ever launched into space [*McMullan et al*., 2008] (Figure 24). MIRAS was developed by a team of 20 companies led by EADS-CASA Espacio. It has 69 elements (66 LICEF and 3 NIR units) distributed along three 4 m long arms, each one including three deployed segments of six elements each, and a central hub with the remaining elements. The spacing between elements is 0.875λ which provides an alias-free field of view of about 400 km and an extended field of view of up to about 1100 km [*Waldteufel et al*., 2003]. The array is tilted 32.5° forward to cover from 0 up to over 50° incidence angle. Observations are performed in full polarimetric mode (but dual-pol is also possible) by sequencing the polarization of the different arms. The basic integration time is 1.2 s. The signals are digitized with 1 bit and over 2500 correlations form a complete set of visibilities. MIRAS includes an onboard calibration system based on the injection of correlated and uncorrelated noise signals. The calibration process also requires external calibrations where the instrument is pointed toward the cold sky. The onboard optical harness for distribution of the reference clock and the routing of the received samples toward the correlator significantly reduces correlation offsets due to potential interfering signals from the instrument.

7. UPC–ICM Contributions to the SMOS Mission

In 1993, the Universitat Politecnica de Catalunya (UPC)–Barcelona started working on what today is the SMOS mission, in an ESA project called "Feasibility Study of a Dual Interferometric Radiometer." This project was devoted to the investigation of the fundamentals of interferometric radiometry for Earth observation and was the starting point of the first of a number of Ph.D. theses on this topic that consolidated our understanding of these techniques [*Camps*, 1996]. Since then, under more than 14 research projects funded by the Spanish government, and more than 36 projects funded by ESA or by companies working for ESA during the development of the SMOS mission, UPC has contributed in a number of aspects to the MIRAS instrument and the SMOS mission, and it is one of the SMOS level 1 Expert Support Laboratories.

These contributions range from instrumental aspects including the development of a simple X band aperture synthesis interferometric radiometer (Figures 25a and 25b) to evaluation of the basic instrument performance (impulse response of the synthetic array, angular resolution, radiometric resolution, radiometric accuracy, and instrument's error budget) and include to the development of sophisticated image reconstruction algorithms (including the Earth-sky and land-sea decompositions to reduce the amplitude of

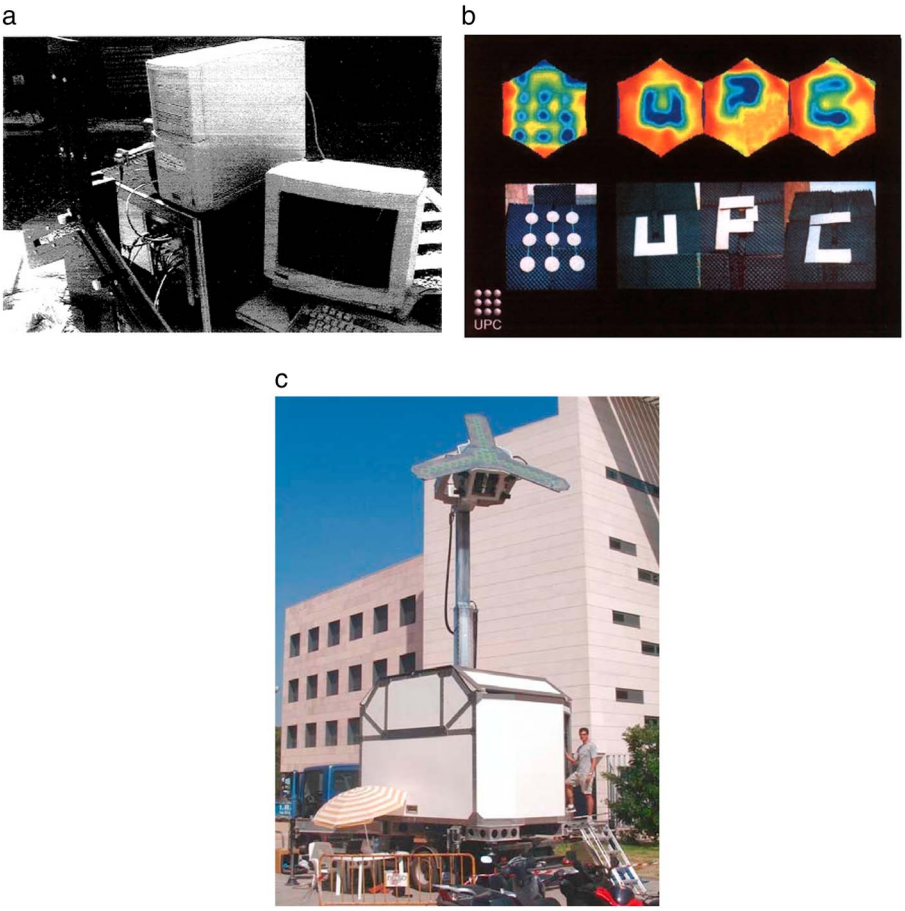

Figure 25. (a) X band dual-antenna demonstrator developed by UPC in 1993–1996 [*Camps*, 1996] and (b) sample composite brightness temperature made from metal plates over microwave absorbers. (c) Dr. Isaac Ramos testing the PAU-SA (synthetic aperture): a fully digital synthetic aperture radiometer to test advanced receiver and calibration techniques developed by UPC in 2006–2012.

the ringing in the coastlines, the Sun cancelation algorithm, or radio frequency interference detection and mitigation algorithms). This work also included the definition of accurate calibration algorithms, including the proposal of a distributed noise injection network instead of a centralized one, and the correlation at different time lags to infer the shape of the fringe-washing function. A previously developed simulator of the MIRAS instrument [*Camps*, 1996] turned out to be a key element of the SMOS mission, when it was upgraded, in conjunction with EADS-CASA Espacio and GMV (Grupo de Mecánica de Vuelo), to become the SMOS End-to-end Performance Simulator. This simulator was used as a test bed to develop soil moisture and ocean salinity retrieval algorithms, and later on the MIRAS Testing Software to test the flight instrument performance. This engineering work was of critical importance, and it is an example of the transfer of know-how from academia to the industrial consortium manufacturing the MIRAS instrument.

In 1998, the scope of the UPC team broadened and joined forces with the Institut de Ciències del Mar–Spanish National Research Council (ICM-CSIC) team, whose leader, Dr. Jordi Font, is the SMOS colead investigator for salinity. The ICM-CSIC team is one of the Expert Support Laboratories for the SMOS level 2 ocean salinity processor development [*Font et al.*, 2010] and has also investigated several aspects of the SMOS image reconstruction procedures [*Gourrion et al.*, 2011]. In 1999–2000 UPC developed the L band Automatic Radiometer (LAURA), a fully polarimetric radiometer designed to operate autonomously in harsh environments in early SMOS-related campaigns. In 2000–2003 the joint team conducted three field experiments, WISE (WInd and Salinity Experiment) 2000 and 2001 in the Casablanca oil rig (Figure 26) and FROG (Foam, Rain, Oil slicks and GPS-reflectometry) 2003 at IRTA (Institut de Recerca en Tècniques Agropecuàries) premises in the mouth of the Ebro River, which were devoted to the study of the emissivity of the sea surface impacted by

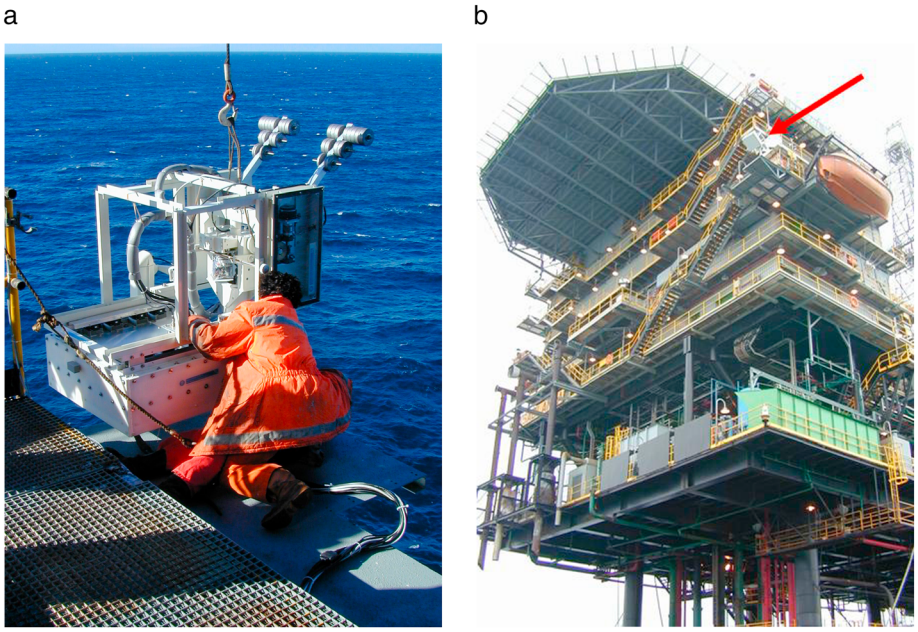

Figure 26. (a) Mounting the LAURA radiometer in the Casablanca oil rig and (b) the LAURA radiometer in the north side of the Casablanca oil rig, as seen from the sea.

the wind, swell, rain, foam, etc. The experimental results were validated with numerical emission models, some developed ad hoc, and were used to test some of the first sea surface salinity retrieval algorithms in the context of SMOS observations. The basic expression used in one of the SMOS roughness models for salinity retrieval is derived from these experiments.

One of the outcomes of the WISE experiments was that the sea state would remain the most difficult variable to correct for in the sea surface salinity retrievals. In this context, in 2003 it was proposed to the European Science Foundation EURopean Young Investigator award to develop the required Global Navigation Satellite Systems Reflectometry (GNSS-R) instrumentation and to perform the required studies to analyze the feasibility of using auxiliary GNSS-R observables to perform this correction without any sea surface height spectrum or any scattering/emission models. This proposal was granted in 2004 [*Camps*, 2004] and led to the development of a suite of hybrid GNSS-R/radiometer instruments under the generic name of passive advanced unit (PAU) that a few years later proved the initial hypothesis [*Valencia et al.*, 2011] while at the same time helped to test new concepts for synthetic aperture radiometers (PAU-SA, Figure 25c).

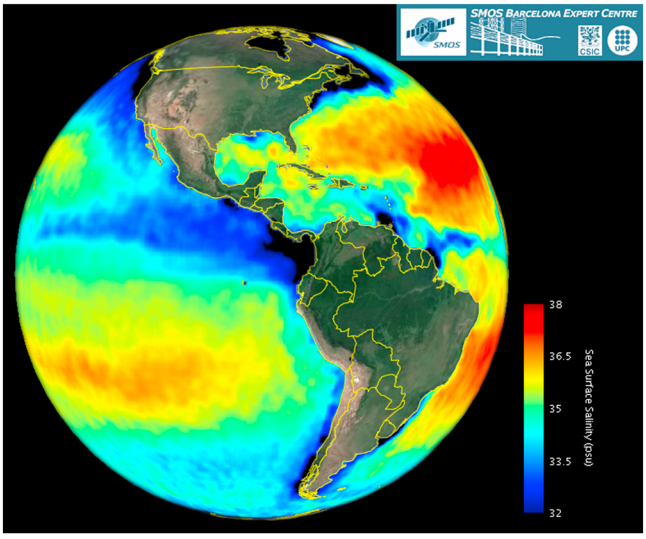

Figure 27. Optimally interpolated global sea surface salinity represented in Google Earth and generated at the SMOS BEC.

In 2003, the LAURA radiometer was deployed in the Valencia Anchor Station to study L band microwave polarimetric emission of grape vines including its azimuthal variation. Since then, LAURA has been deployed in more than eight field experiments to address the impact of the main variables governing soil emissivity at L band (i.e., soil moisture, soil texture, soil surface roughness, presence of vegetation canopies, and

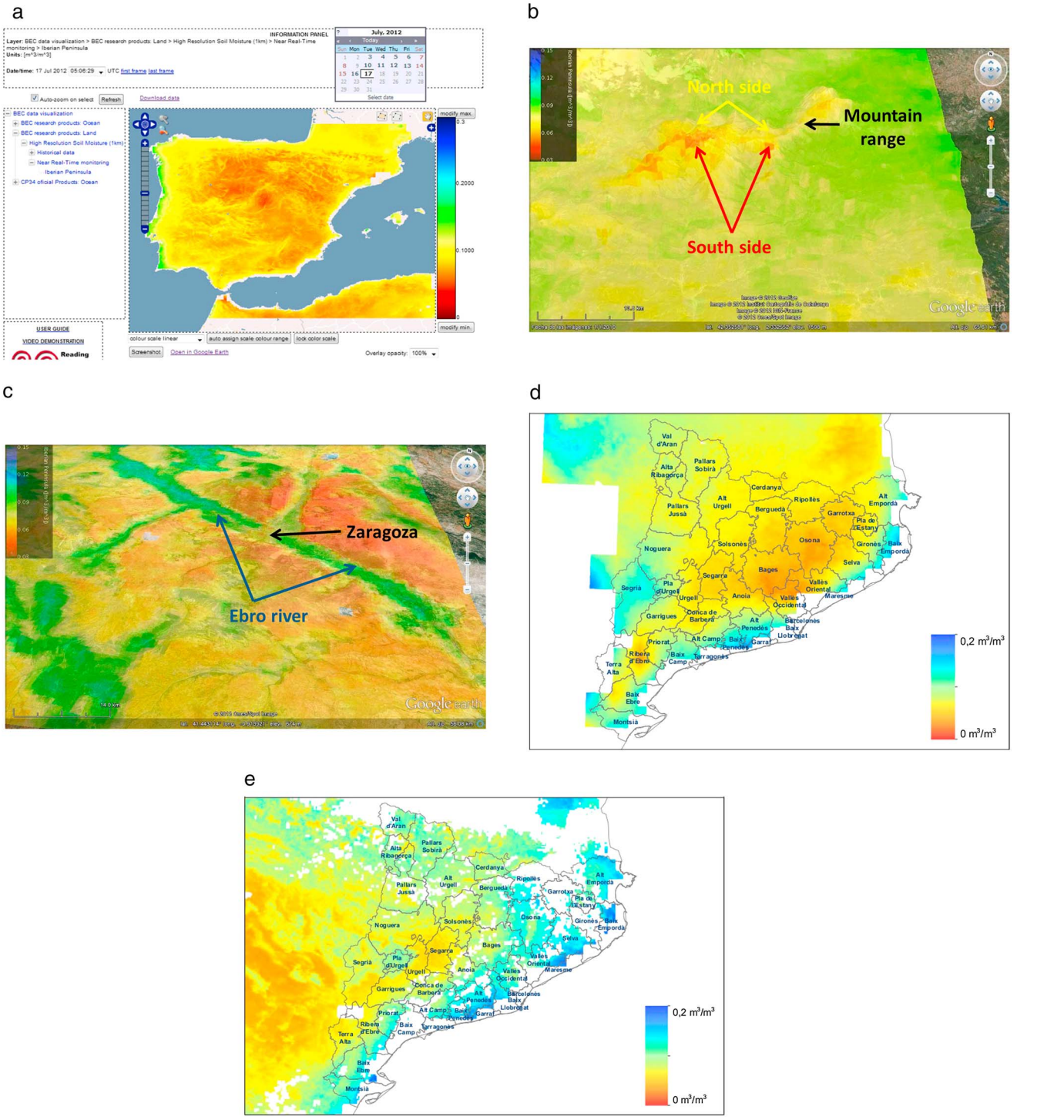

Figure 28. (a) Downscaled 1 km soil moisture map of the Iberian Peninsula corresponding to 17 July 2012. (b) Zoom over the Pyrenees: note the northern sides of the mountains are wetter than the southern ones. (c) Zoom over the Ebro River, as it flows through the city of Zaragoza. Note the larger moisture values along the Ebro River and its tributaries. (d) Downscaled 1 km soil moisture map of Catalonia of 8 July 2012 at 4:30 h, and (e) at 16:30 h. Note the change in soil moisture due to a rain event. Missing pixels are due to the presence of clouds and the lack of MODIS data.

topography). To support the SMOS validation activities, from November 2008 until May 2010 LAURA was deployed in the REMEDHUS (Red de Estaciones de MEDición de la HUmedad del Suelo) site (province of Zamora, Spain) on a long-term field experiment. All these results have contributed to a better characterization of the L band soil emissivity models that are used in the SMOS soil moisture retrieval algorithms. Additionally, data fusion algorithms that combine microwave measurements with multispectral VIS-NIR data were developed with the aim of increasing the spatial resolution of the soil moisture retrievals. These methods were first applied from a remote-controlled aircraft, and after the launch of SMOS they been used to successfully combine MIRAS/SMOS radiometric measurements (~50 km pixel) and Moderate Resolution Imaging Spectroradiometer (MODIS) Terra/Aqua temperature and vegetation parameters into 1 km soil moisture maps (Figure 28) [*Piles et al*., 2011].

In 2007, the SMOS Barcelona Expert Center (SMOS-BEC) was founded to foster the cooperation between ICM/CSIC and UPC in SMOS and other remote sensing activities, by taking advantage of a powerful computing infrastructure granted by the Spanish Ministry of Science and Innovation. The SMOS-BEC is also responsible for the scientific aspects of the CP34 (Spanish SMOS levels 3 and 4 data processing center). In addition to the official ESA SMOS products that cover up to level 2, the CP34 provides new added-value research products (e.g. http://cp34-bec.cmima.csic.es/youtube), such as optimally interpolated sea surface salinity (Figure 27), fused with other remotely sensed sea surface data, or the 1 km soil moisture data over the Iberian Peninsula that are routinely produced in near real time (Figures 28a–28c). Figures 28d and 28e show an example of a SMOS morning and afternoon overpass over Catalonia. The change in soil moisture associated with a rain event that happened in the middle of the day is clearly visible. During summer 2012, these near real-time maps have been distributed daily to the Catalonian firemen headquarters to help detecting extremely dry soil and vegetation posing a risk of fire. These products can be freely downloaded from links (http://cp34-bec.cmima.csic.es/) and (http://cp34-bec.cmima.csic.es/NRT). The interested reader is also referred to *Camps et al*. [2012] and the web links (http://www.icm.csic.es/oce/), and (http://www.tsc.upc.edu/rslab/Passive%20Remote%20Sensing/Welcome).

8. Developments in Helsinki University of Technology

8.1. Background

The Remote Sensing Group of Helsinki University of Technology (HUT, part of Aalto University, Espoo, since 2010) has been developing microwave radiometers and their remote sensing applications since the 1970s. Conventional single-frequency radiometers operating at UHF and microwave bands up to 37 GHz were constructed and used for developing cryospheric applications including sea ice, snow, forest, and peat. Initially, data were acquired with tower-based and helicopter-borne measurements; however, this only allowed collection of local data sets. A twin-engine turboprop aircraft, Short SC 7 Skyvan, was acquired in 1994 and subsequently modified for remote sensing research. With a dedicated platform available for instrumentation, construction of our first multifrequency radiometer system was readily completed, and it was used in the ESA European Multisensor Airborne Campaign on snow and sea ice carried out in northern Finland in 1995. Later the airborne 6.9–94 GHz radiometer system Helsinki University of Technology Radiometer (HUTRAD) was completed, and it has been used for multiple applications over the years. Airborne radiometer measurements were considered a useful tool for developing applications and testing new instrument concepts, and consequently, new opportunities were sought in the middle 1990s.

8.2. HUT-2D Aperture Synthesis Radiometer

The HUT Group carried out a preliminary study in 1996 of new microwave radiometer techniques including a 1.4 GHz aperture synthesis radiometer and a 36.5 GHz polarimetric radiometer. Subsequently, both radiometers were realized. Design of an airborne L band aperture synthesis radiometer was started in 1997–1998 in collaboration with Finnish industry, whose responsibilities included the design and manufacturing of the radio frequency (RF) and intermediate frequency (IF) subsystems, while overall system design, antennas, integration, and testing were covered by HUT. The system was designed to consist of 36 antenna/receiver modules, whose in-phase and quadrature outputs are correlated with a 1 bit digital correlator. For each subgroup of four receivers, there is a local oscillator and a calibration unit. The instrument was originally planned to be accommodated around the rear door of the Skyvan aircraft in a U-shaped geometry. For easier accommodation, the plan was

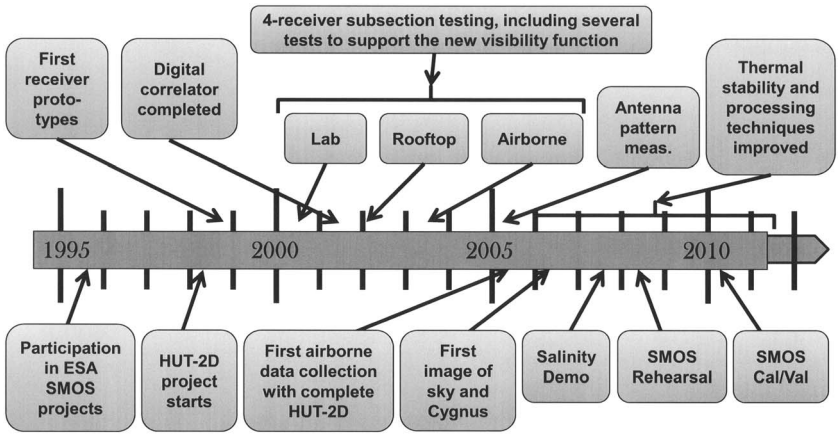

Figure 29. Major milestones in the development and use of the HUT-2D aperture synthesis radiometer [after *Kainulainen et al*. 2011b].

changed and the system was mounted below the fuselage of the aircraft, maintaining the geometry. The first prototypes of the receivers and the calibration systems were completed in 1998. Then the collaborating industry withdrew from the project, and the HUT Group assumed responsibility for the design and construction of the whole radiometer including the receivers.

In the design of the receiver, special attention had to be paid to the problem of coupling and overhearing between the radiometer channels. Several versions of the layout of the RF and receiver control board (RCB) were produced until the design was frozen. Considerable effort was devoted to electromagnetic compatibility (EMC) shielding of the various sections of the RF and RCB boards including EMC testing of the four-receiver subsection in the laboratory, on a rooftop and while airborne. The four-unit subsystem was flown in December 2003 with proper performance behavior [*Rautiainen et al*., 2008]. The first airborne data acquisition with the complete HUT-2D system was conducted in May 2005 demonstrating the system's capability to produce interferometric data [*Kainulainen et al*., 2007]. Figure 29 depicts major milestones in the development of the HUT-2D system ranging from our first participation in an ESA SMOS-related project in 1995 to the ESA SMOS Cal/Val airborne campaign in 2010. The technical characteristics of HUT-2D are shown in Table 1. The radiometer provides a swath of 95% of the flight altitude, 14×15 pixels within the alias-free field of view, and an angular resolution of 3 to 6° depending on tapering. Figure 30 shows a photo of the Skyvan aircraft with the HUT-2D system (size 2 m by 2 m, weight 100 kg) mounted below the fuselage.

The HUT-2D system has been a key element for the preparation and execution of the SMOS mission including the following highlights: (a) the SMOS onboard calibration system was first tested on the HUT-2D radiometer; (b) the Corbella equation, which provides the theoretical basis for remote sensing by aperture synthesis, was verified using HUT-2D; (c) the SMOS external calibration strategy was verified by the first ever image of galaxy acquired by an SMOS-like interferometer; (d) the HUT-2D instrument on board Skyvan provided the first end-to-end demonstration of the SMOS mission concept; (e) the first ever SMOS-like sea surface salinity retrievals were made by HUT-2D; and (f) HUT-2D on board the Skyvan was used to acquire airborne data for selected test sites in the ESA SMOS 2008 Rehearsal Campaign and the 2010 Cal/Val Campaign.

The HUT-2D system has been in operational use since 2006. The performance of the HUT-2D radiometer has been analyzed in detail based on measurements of well-known natural targets, such as cosmic background radiation and low-salinity water scenes [*Kainulainen et al*., 2011a].

8.3. Contributions to the Design and Characterization of MIRAS

Along with the construction of the HUT-2D radiometer, the HUT Group participated in various projects in preparation and support of the SMOS mission including implementation of the MIRAS on board Calibration System (CAS) in the HUT-2D in 1998 and, together with Ylinen Electronics Ltd., development of the CAS of

Table 1. Technical Characteristics of the HUT-2D Radiometer

Parameter	Value
Center frequency	Nominal 1413 MHz, adjustable within 1400 to 1427 MHz
Bandwidth	7 MHz
Polarization	Switchable dual linear polarisations
Alias-free field of view	± 25°
Swath	0.95 x altitude
Boresight pointing	Nadir
Radiometric sensitivity	0.8 K (integration time 4000 ms) 2.8 K (integration time 250 ms)
Angular resolution at boresight	3° (no tapering) 4° (triangular tapering) 6° (Blackman tapering)
No. of pixels within the alias-free field of view	14 × 15
Minimum incidence angle	0° (vertical)
Maximum incidence angle (center of pixel fully in alias-free field of view with maximum incidence angle)	34° for pixels in image corner 23.5° for pixels in image linear axes

MIRAS in 1999–2000. A major effort was the development of the Noise Injection Radiometer (NIR) and additional CAS hardware in 2001–2005. The NIR measures the average scene brightness temperature for absolute calibration of the MIRAS image map and the noise temperature level of CAS. The HUT Group characterized both the NIR and CAS systems in 2002–2006 [*Colliander et al*., 2007; *Lemmetyinen et al*., 2007] with these data were later included in the MIRAS Data Base and used by the SMOS level 1 data processor. The results of a recent study conducted with a full year of data indicate that the NIR units are operating well within the requirements. The radiometric resolution of the units is on the order of 0.20 K, as expected [*Kainulainen et al*., 2012].

8.4. Contributions to GNSS-R and RFI Studies

Global Navigation Satellite System Reflectometry (GNSS-R) is a potential tool for characterizing sea surface roughness that is a major obstacle in retrieval of salinity from L band radiometer data. In *Kainulainen et al*. [2011c] a new correlation is introduced between the mean square slope measured using GNSS-R and the first Stokes parameter measured by L band radiometry. The retrieved correlation was used to establish a linear model to estimate the roughness component of sea emission, which was further used in comparison with the HUT-2D measurements. The derived model was compared with two other models based firmly on the earlier WISE experiment carried out in the Mediterranean Sea. The good correlation of the model with the radiometric measurement shows the potential of the GNSS-R technology.

Figure 30. The U-shaped HUT-2D radiometer is accommodated below the fuselage of the Skyvan aircraft, and the HUTRAD multifrequency radiometer is in the rear compartment with the back door removed. The two systems cover a frequency range of 1.4 to 94 GHz. Photo courtesy of Jaakko Seppänen.

It was recently demonstrated [*Hallikainen et al*., 2011] using data collected with the airborne HUT-2D as well as with the spaceborne MIRAS instrument that point-like RFI has severe impacts on the imaging area of the radiometers, even when the RFI is not physically located in the usable alias-free imaging area of the instrument.

9. Developments at the National Space Science Center

9.1. A Historical Review

The Center for Space Science and Applied Research (CSSAR), Chinese Academy of Science (CAS), is located in Beijing (China). The microwave remote sensing technology laboratory within CSSAR is a key laboratory of CAS and has a team dedicated for synthetic aperture radiometer development. The name of CSSAR was changed to National Space Science Center (NSSC) in the summer of 2011.

The development started in the summer of 1996 during Dr. Ji Wu's visit as a visiting scholar at the Microwave Remote Sensing Laboratory (MIRSL) of University of Massachusetts at Amherst. Dr. Wu worked with Professor Calvin Swift during his stay in Amherst. They discussed many key issues of this technology, particularly on instrument noise.

After Dr. Wu came back to Beijing, he started his own group, initially working on a digital correlator. The experiments successively demonstrated the principle of a 2 bit correlation of two coherent receiving channels. After that, he used this correlator to measure a point source and drew an interference pattern with I and Q outputs. Before development of a full instrument, but using this correlator and by changing the baseline, he also achieved a full-coverage time-shared measurement of the spatial frequency domain spectrum. The point source location was then obtained by Fourier transformation.

The first full instrument developed at NSSC by Wu's team is a C band six-element/channel one-dimensional synthetic aperture radiometer with a spatial resolution of 4° [*Zhang et al*., 2002]. The instrument is very much like ESTAR developed by MIRSL, with a slotted waveguide element antenna array, mounted below the instrument box and installed outside of the helicopter. The fan beam of each element antenna is in the cross-track direction. Therefore, the synthetic aperture resolution is obtained only in the cross-track direction. In the along-track direction, the resolution is obtained by the real aperture of the element antennas. Before the instrument was mounted on the helicopter, it was first calibrated by looking at the cold sky. It was then flown on board a helicopter over the Yellow River in Shan Xi Province in China. This instrument was a great encouragement to the team. A 4° spatial resolution image over the Yellow River was retrieved. The water and land boundaries and also the islands in the river were clearly identified. The image was used for soil moisture retrieval and presented in International Geoscience and Remote Sensing Symposium (IGARSS) in 2003 [*Zhang et al*., 2003].

The follow-on development was an X band eight-element/channel one-dimensional synthetic aperture radiometer. For experimental and redundant reasons, the instrument has two correlators. One is analog, the other is digital. The spatial resolution of this instrument is less than 2°. At the boresight direction, the resolution is in fact about 1.8°. As the C band instrument, it was also flown on board of a helicopter. The measurements were carried out in the northeast of China over Jingpo Lake and Songhua Lake. The noise of this instrument is much less than the previous one due to updated front-end electronics. The image obtained by this instrument is also better than the previous one. The ice and water of the lake could be clearly identified. The calibration of the instrument is the same as before (i.e., looking at the cold sky before the instrument is mounted on the helicopter prior to each flight). The design and measurement results were presented in IGARSS in 2004 [*Liu et al*., 2004].

A further study of one-dimensional synthetic aperture concentrated on a X band fully polarized interferometric radiometer (FPIR). Two sets of waveguide arrays of orthogonal polarizations share the same physical aperture and produce images in two polarizations. Each element antenna has a conical beam in order to have the same incident angle across the footprint on the ground. A ground demonstrator of FPIR was tested and first ever images of buildings in dual polarizations were acquired.

In parallel to the one-dimensional synthetic aperture radiometer development, there was also basic research of this technology. It is the time-shared scan technology. As long as the future of the synthetic aperture radiometer is concerned, there will be 1 day that the instrument becomes so complicated that the overall weight and complexity become unacceptable. For this reason, the team has been looking for ways to reduce the complexity. One possible way is to use time-shared sampling scheme. The so-called time-shared scan means samples are taken in the spatial frequency domain in a time-shared way instead of a snap shot. However, this method can only be used in the case that the scene is invariant during the time that

the measurement is carried out. For moving target or fast-moving platform, the time-shared scan cannot be used.

A successful development of the time-shared measurement is illustrated with a rotating scan array. In this array, the element antennas are placed on a circle. The positions of each element antenna are calculated and optimized in a way that the lengths of the baselines they form are not redundant. This means that they all have different lengths from 0 to a maximum u and uniformly distributed. Since the element antennas are placed on a circle, the directions of the baselines must be different. However, if the circle rotates around its center, the sampling points in the spatial frequency domain will then have a full coverage [*Wu et al*., 2007].

9.2. The Geostationary Interferometric Microwave Sounder

This recent instrument development is an application of the rotation scan technology. The instrument, named GIMS (Geostationary Interferometric Microwave Sounder), is a full-scale demonstrator dedicated to a geostationary meteorology satellite. The working frequency is from 50 to 60 GHz with eight bands. The system has 28 elements placed on a circle of 2.8 m in diameter. The position of each of element antenna is optimized covering all baselines uniformly distributed from 0 to the longest baseline. During the measurement, the instrument rotates. Each image needs only a 180° rotation. The specification is for an image refresh time of 5 min. Therefore, the rotation speed is about one turn every 10 min or six revolutions per hour. The Earth surface resolution of this instrument is about 50 km from geostationary orbit. Since clouds will not move fast within 50 km, the refresh time of an image in 10 min is acceptable. Therefore, the use of time-shared or rotation scan can significantly simplify the instrument. It is hard to imagine how many element/channels a snapshot instrument with similar specifications should have, not to mention the weight and power it would require.

Figure 31 shows a photo of the GIMS demonstrator and its image of a building and three people, two of them were holding a metal plate. One of the plates is big and the other is small. In the image, the building, the people, and the metal plates are all seen quite well. This demonstrator provides a solid base for the engineering phase of the instrument for a Chinese geostationary meteorology satellite.

9.3. Clock Scan and SPORT Mission

Along the direction of rotation scan or time-shared scan, NSSC has carried out another study searching for the way to use the least number of element antennas or receiving channels. In the extreme case, the number of element antennas or receiving channels can be reduced down to two. This results in an increased scanning time for the full image. In this case, the two-element antennas should be mounted on the far end of two clock arms. The two clock arms rotate at different speeds. Classically, once the second arm makes a full rotation, the minute arm rotates by one step only. In practice, as long as the two arms rotate at different speeds, the u-v plane will be fully sampled. Therefore, this method is simply being called the "clock scan" [*Wu et al*., 2007].

The sensitivity of the two-element clock scan is a consideration. Since the sensitivity of the radiometer system depends on both the integration time and energy received by the element antennas, the two-element clock scan system will have the worst sensitivity. In order to increase the sensitivity of the clock scan system, the $2+2$, $4+4$, … …, $n+n$ element-system can be considered. For example, in the $4+4$ system, there are four second arms and four minute arms, as shown in Figure 32. This reduces the scan/sampling time by comparison with the two-element system. Such a system has been proposed for a space mission called SPORT (Solar Polar Orbit Radio Telescope), which looks the interplanetary corona mass ejections from solar polar orbit [*Wu et al*., 2011].

As long as the rotation scan is considered, no matter whether it is a single rotation of a circular array or the clock scan, the classic Fourier transformation is not valid anymore. A numerical method should be used to interpolate the sampling points to a grid where the Fourier transformation can be applied. For the circular-type sampling points, the most suitable method should be the pseudopolar grid-based fast Fourier transformation.

The pseudopolar FFT method is particularly suitable for the polar grid-type of data. Using two steps of 1-D interpolations, the angular interpolation and radial interpolation, the polar grid can be converted to a pseudopolar grid, which is composed by concentric rectangles and equisloped rays. Then applying 1-D FFT

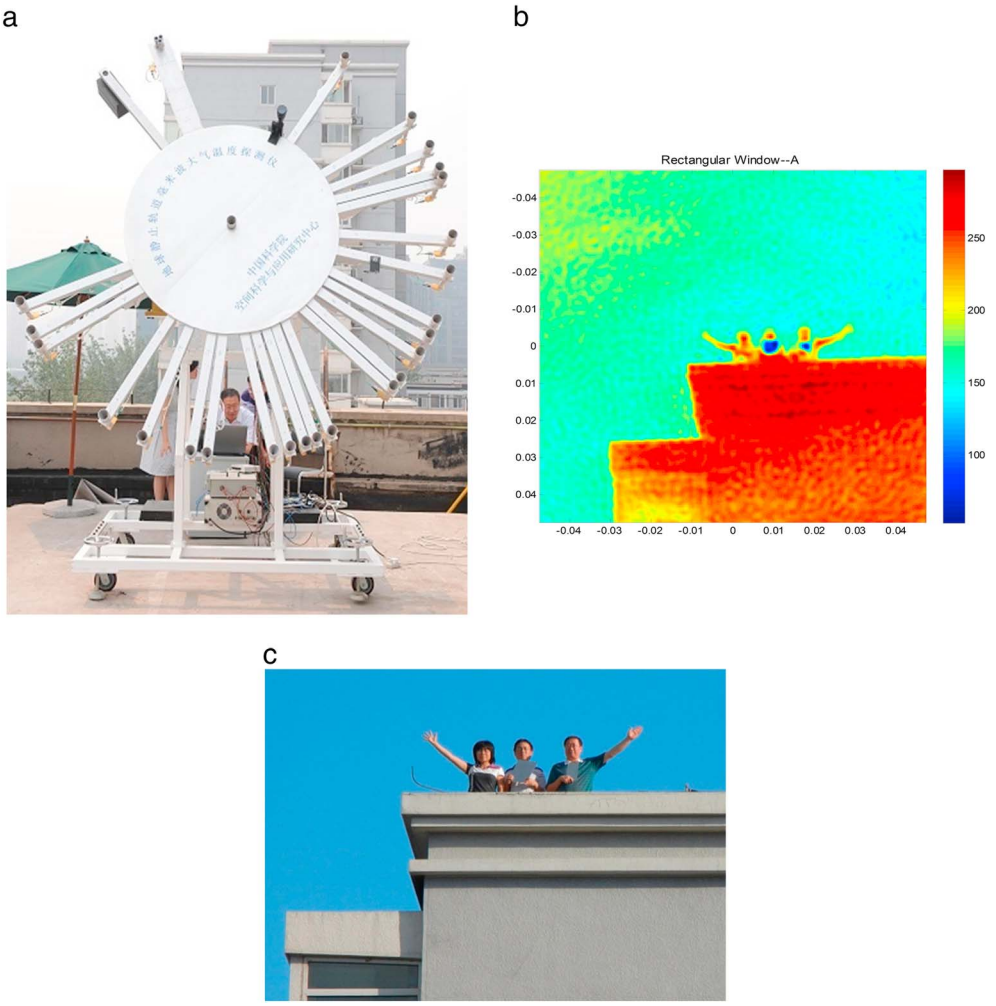

Figure 31. (left) Full-size demonstrator for geostationary sounder. (middle) Retrieved image. (right) Original scene taken by charge-coupled device camera [see *Zhang et al.*, 2012].

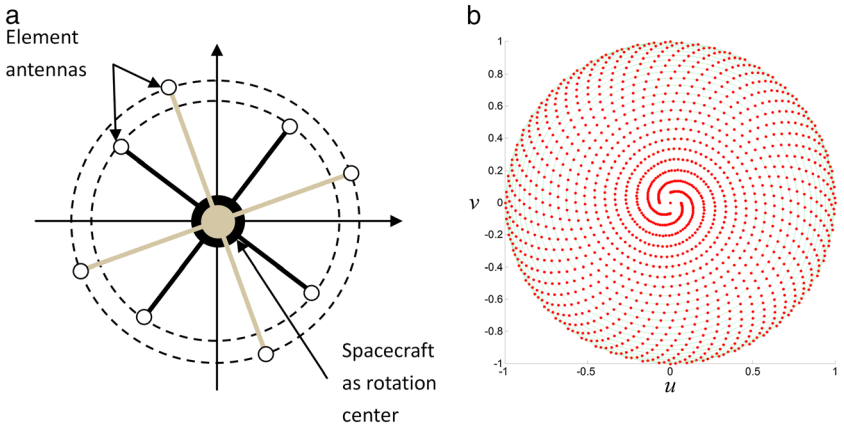

Figure 32. The 4 + 4 clock scan setup and its sampling in the u-v plane.

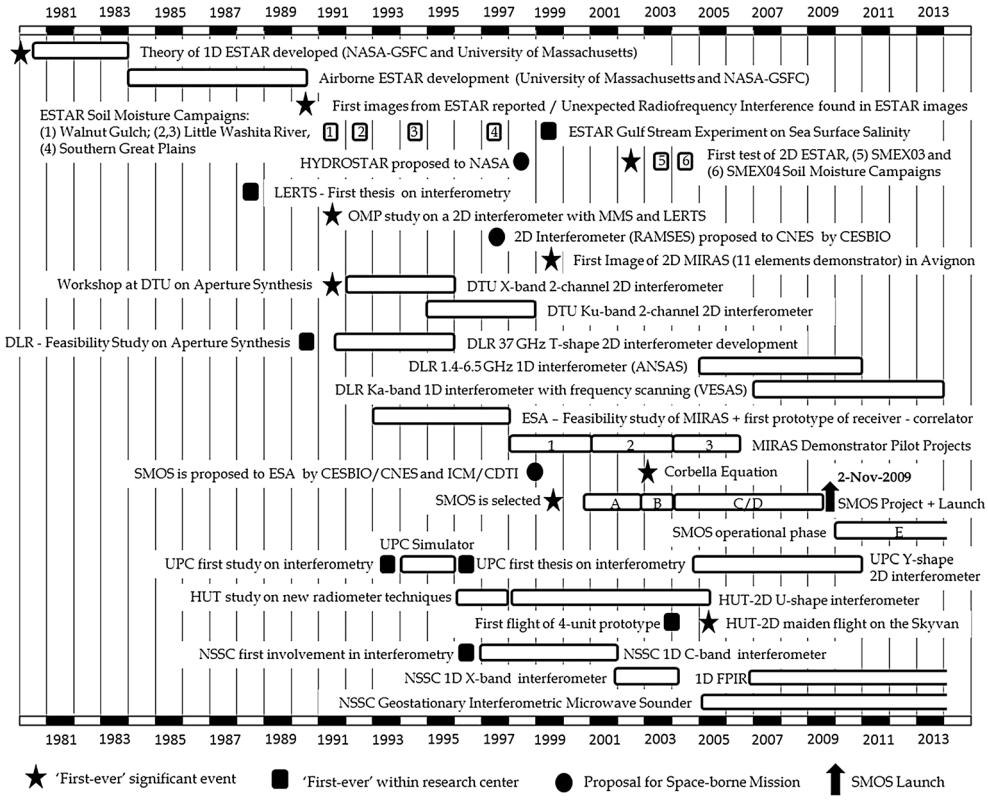

Figure 33. Time line of the main developments in aperture synthesis up to the launch of SMOS. Main contributing centers were, in chronological order, NASA-Goddard Space Flight Center (GSFC, US), CNES-Centre d'Etudes Spatiales de la Biosphère (CESBIO, France), Technical University of Denmark (TDU, Denmark), Deutsches Zentrum für Luft- und Raumfahrt (DLR, Germany), European Space Agency (ESA, Europe), Polythecnic University of Catalonia (UPC, Spain), Aalto University (formerly Helsinki University of Technology–HUT, Finland), and the National Space Science Center (NSSC, China).

and fast FRFT (fractional Fourier transform), the circularly or spiral type of sampling points can be transformed to a Cartesian grid in the spatial domain. The interpolation pseudopolar FFT method has a promising performance due to high accuracy of 1-D interpolations and fast computational operations compare with other methods used in this particular circular sampling data.

The studies of the rotation scan, in particular the clock scan, and its associated image-retrieving method, provided a new approach for the interferometric or synthetic aperture radiometer development. While the snapshot systems become more and more complicated systems with hundreds, or even thousands of channels, NSSC tried to use the lowest number of channels (two) and build up from there. This allows engineers to design the simplest system with the minimum number of channels as long as the sensitivity requirement can be achieved and the observed scenes are not fast-moving targets.

10. The Future

10.1. Open Challenges

Even 4.5 years after the launch of SMOS, we are still learning from the in-flight data. On the one hand, we have consolidated our knowledge on how microwave interferometric radiometry really works in practice by explaining many of the features seen in SMOS images. On the other hand, we know now quite well what things could be improved if we were to build an instrument similar to MIRAS for a future mission.

The main open challenges for a future SMOS mission are (a) improvement of the spatial resolution (must be a real quantum step down to 3–10 km); (b) robustness against RFI; (c) better temporal resolution, for land applications in particular, from 3 days revisit to twice daily, to capture the diurnal cycle not only at global but also at regional scales; (d) additional observation of sea state (surface roughness) for improved sea surface

Table 2. SMOSops Predicted Performance

Parameter	SMOSOps-H	SMOS
Diameter	6.5 m	8 m
Element spacing	0.767λ	0.875λ
Number of antennas per arm	20	21
Total number of antennas	120	69
Number of baselines	7140	2346
Tilt angle	21°	32.5°
Steering angle	30°	30°
AF-FOV swath	946 km	587 km
Polarization	full-pol	full-pol (effectively)
Image resconstruction window	Blackman	Blackman
Number of u-v points	4921	2791
Synthetic beam side-lobe level: (ξ plane)	−28.4 dB	−14.3 dB
(η plane)	−27.08 dB	−16.7 dB
Synthetic beam −3 dB beamwidth	2.22°	2.26°
Spatial resolution at boresight	33.0 km	40.6 km
Receiver noise temperature	150 K	210 K
Sampling rate	115.39 MHz	55.85 MHz
Effective integration time	0.70	0.66
Redundancy factor	0.69	0.94
Snapshot radiometric sensitivity (SM) at boresight	1.22 K	2.37 K
Snapshot radiometric sensitivity (OS) at boresight	0.84 K	1.73 K
Effective radiometric sensitivity (SM) at FoV center	0.11 K	0.40 K
Effective radiometric sensitivity (OS) at FoV center	0.07 K	0.29 K

salinity retrievals; (e) measurements of all four Stokes parameter simultaneously to simplify conversion from brightness temperatures from antenna to Earth frame and to further improve RFI detection; (f) reduce image noise floor and improve precision, in particular important over ocean and coastal areas, and (g) cost effective instrument design ready for integration into operational satellite systems.

These points are addressed in presently investigated follow-on or next generation SMOS-type mission concepts, such as SMOS operational follow-on mission (SMOSops) by ESA and SMOS-NEXT (Soil Moisture and Ocean Salinity NEXT generation) by CNES.

10.2. SMOSops

SMOSops is intended as an operational mission based on and to follow SMOS, and aimed at providing scientists with continued high-resolution SM and SSS observations with improved accuracy. Table 2 shows the predicted performance for SMOSops by comparison to that of SMOS [*Zurita et al.*, 2013]. SMOSops addresses all aspects mentioned above except for (a), as its spatial resolution is similar to that of SMOS. The robustness against RFI (b) is to be achieved by the use of a hexagon-shaped array, which should focus RFI energy better without sidelobe tails. The shorter revisit time (c) is achieved by a larger field of view thanks to a reduced spacing between antenna elements. The observation of sea surface roughness (d) is proposed through the use of GNSS reflectometry (an additional passive payload which would be added to the platform). The improved radiometric accuracy (f) is obtained by a combination of several enhancements: the use of an hexagon shape (instead of a Y) which leads to lower sidelobes, the parallel measurement of all four Stokes parameters addressed in (e), the much wider alias-free field of view (hence many more snapshots along incidence angle), an increased sampling rate, a larger antenna ground plane (to reduce backlobes) with an improved thermal design (to reduce orbital and seasonal variations). In particular, the estimated improvement in effective sensitivity is fourfold with respect to that of SMOS.

It is noted that SMOSops would be far more robust against RFI (thanks to its lower side lobes) and against receiver failure (thanks to its degree of redundancy, two in all visibilities compared to only one in SMOS). The deployment of a hexagon-shaped array has been cleverly solved by the use of running cone hinges.

10.3. SMOS-NEXT

After the successful launch of SMOS, Aquarius was also successfully launched on 10 June 2011 and SMAP (Soil Moisture Active and Passive) is scheduled for launch in November 2014. These missions are in a way very

complementary to SMOS and should also bring new results together with new challenges. New work certainly will address intercomparison of these instruments and synergisms with other sensors either in the optical/thermal infrared range or with active/passive microwave sensors. But the lingering challenge is still there. How to achieve a good temporal and spatial sampling of the globe for soil moisture and sea surface salinity? The simplest approach relies on the so-called disaggregation techniques. It relies on the use of high-resolution sensors to distribute soil moisture as measured by an interferometer. Very successful results have been already gained [*Merlin et al*., 2005, 2010, 2012]. SMAP will address also the issue by merging active and passive measurements. However, these approaches also have limitations (cloud cover, data availability, or, more challenging, validity domains). CNES has thus initiated new research activities whose goals is to develop a new mission which would fulfill all the SMOS requirements but with 10 times better spatial resolution and an improved sensitivity (factor of 3 for salinity applications) paving the way to more applications in water resources management, coastal area monitoring, basin hydrology, or even thin sea ice monitoring [*Kaleschke et al*., 2012]. The concept, named SMOS-NEXT, is based of merging spatial and temporal 2-D interferometry and is currently undergoing phase 0 at CNES with a proof of concept experiment funded by the Research and Development program.

Acknowledgments

The following people are acknowledged for having had important contributions, one way or another, to the developments presented in this paper: Jean-Marc Goutoule (Astrium EADS, Toulouse), Calvin Swift (Amherst), Achim Hahne (ESA), Kevin McMullan (ESA), Francesc Torres (UPC), Nuria Duffo (UPC), Veronica Gonzalez (UPC), Mercé Vall-llossera (UPC), Josep Closa (ECE), Roger Oliva (ESA), Fernando Martin-Porqueras (IDEAS), André Lannes (OMP), Jean-Pierre Wigneron (EPHYSE), Eric Anterrieu (IRAP), François Cabot (CESBIO), Philip Waldteufel (LATMOS), Chris Ruf (University of Michigan), Alan Tanner (JPL), Bill Wilson (JPL), Brian Laursen (DTU), Matthias Jirousek (DLR), Eric Schreiber (DLR), Kimmo Rautiainen (FMI), Juha Kainulainen (HUT), Tuomo Auer (HUT), Jorgen Pihlflyckt (HUT), Simo Tauriainen (HUT), Andreas Colliander (JPL), Juha Lemmetyinen (HUT), Janne Lahtinen (Harp Technologies), Serni Ribo (IEEC), Hao Liu (NSSC), Jingye Yan (NSSC), Cheng Zhang (NSSC), and Weiying Sun (NSSC). There are many other people who would also deserve to be included here. For them goes this acknowledgment too.

References

Anterrieu, E. (1992), Synthèse d'ouverture multi-pupillaire: Algorithmique de reconstruction d'image, PhD problèmes inverses de reconstruction d'image, Université Paul Sabatier, Toulouse, France.

Assad, E., J. P. Fréteaud, Y. H. Kerr, J. P. Lagouarde, and B. Seguin (1986), Utilisation de la thermographie infrarouge dans l'estimation de l'évaporation à l'échelle régionale: Application au sénégal, *Agronomie Tropicale*, *40*(4), 279–285.

Bayle, F., et al. (2002), Two-dimensional synthetic aperture images over a land surface scene, *IEEE Trans. Geosci. Remote Sens.*, *40*(3), 710–714.

Blanchard, B. J., M. J. McFarland, T. J. Schmugge, and E. Rhoades (1981), Estimation of soil-moisture with API algorithms and microwave emission, *Water Resour. Bull.*, *17*(5), 767–774.

Camps, A. (1996), Application of interferometric radiometry to Earth observation, PhD thesis dissertation, Universitat Politècnica de Catalunya Advisors: I. Corbella, J. Bará. [Available at http://www.tdx.cat/handle/10803/6885.]

Camps, A. (2004), "Passive advanced unit (PAU): A hybrid L-band radiometer, GNSS-reflectometer and IR-adiometer for passive remote sensing of the ocean," Project Description EURYI 2004 awards. [Available at http://www.esf.org/activities/euryi/awards/2004.html], last visited: November 6th 2012.

Camps, A., et al. (2012), Review of the CALIMAS team contributions to European Space Agency's soil moisture and ocean salinity mission calibration and validation, *Remote Sens.*, *4*, 1272–1309.

Chanzy, A., T. J. Schmugge, J. C. Calvet, Y. Kerr, P. vanOevelen, O. Grosjean, and J. R. Wang (1997), Airborne microwave radiometry on a semi-arid area during hapex-sahel, *J. Hydrol.*, *189*(1-4), 285–309.

Choudhury, B. J., Y. H. Kerr, E. G. Njoku, and P. Pampaloni (1995), Passive microwave remote sensing of land-atmosphere interactions, VSP.

Colliander, A., L. Ruokokoski, J. Suomela, K. Veijola, J. Kettunen, V. Kangas, M. Levander, H. Greus, M. Hallikainen, and J. Lahtinen (2007), Development and calibration of SMOS reference radiometer, *IEEE Trans. Geosci. Remote Sens.*, *45*(7), 1967–1977.

Corbella, I., N. Duffo, M. Vall-llosera, A. Camps, and F. Torres (2004), The visibility function in interferometric aperture synthesis, *IEEE Trans. Geosci. Remote Sens.*, *42*(8).

Corbella, I., F. Torres, N. Duffo, A. Camps, M. Vall-llossera (2008), *Brightness Temperature Retrievals from the Small Airborne MIRAS*, vol. 2, 649–652, IEEE International Geoscience and Remote Sensing Symposium, IGARSS 2008, Boston (MA) 6-11 July, doi:10.1109/IGARSS.2008.4779076.

Daganzo-Eusebio E., R. Oliva, H. K. Yann, S. Nieto, P. Richaume, S. Mecklenburg (2013), SMOS radiometer in the 1400–1427 MHz passive band: impact of the RFI environment and approach to its mitigation and cancellation, *IEEE Trans. Geosci. Remote Sens., 51*(10), 4999–5007.

Eagleman, J. R. L., and W. C. Lin (1976), Remote sensing of soil moisture by a 21 cm passive radiometer, *J. Geophys. Res.*, *81*, 3660–3666, doi:10.1029/JC081i021p03660.

Engman, T., D. M., LeVine, Y. Kerr, P. Waldteufel, M. Martín-Neira (1998), White paper on Aperture Synthesis Technology Road Map for Observation of Soil Moisture and Ocean Salinity, NASA Goddard Space Flight Center, 13-14 July.

Font, J., A. Camps, A. Borges, M. Martín-Neira, J. Boutin, N. Reul, Y. H. Kerr, A. Hahne, and S. Mecklenburg (2010), SMOS: The challenging Sea surface salinity measurement from space, *Proc. IEEE*, *98*(5), 649–665.

Goodman, J. W. (1985), *Statistical Optics*, John Wiley, New York.

Gourrion, J., R. Sabia, M. Portabella, J. Tenerelli, S. Guimbard, and A. Camps (2011), Characterization of the SMOS instrumental error pattern correction over the ocean, *Geosci. Remote Sens. Lett., IEEE*, *9*(4), 793–797, doi:10.1109/LGRS.2011.2181990.

Goutoule, J. M., E. Anterrieu, Y. H. Kerr, A. Lannes, and N. Skou (1996), MIRAS microwave radiometry critical technical development, TOULOUSE, MMS.

Greiner, M., M. Peichl, H. Süß (2003), Advanced image reconstruction and array geometries in aperture synthesis radiometry, Proc. of IGARSS'03, International Geoscience and Remote Sensing Symposium 2003, Toulouse, France, 21-25 July.

Grüner, K., G. Kahlisch, H. Schreiber, P. Sliwinski, and B. Vowinkel (1992), A new passive microwave line scanner for airborne measurements of maritime oil pollutions, IEEE-MTT Conf., Albuquerque, N. M.

Hallikainen, M., J. Kainulainen, J., Seppänen, K. Rautiainen (2011), Investigation of radio frequency interference at using data from airborne HUT-2D radiometer and spaceborne SMOS radiometer, paper presented at XXX URSI General Assembly and Scientific Symposium, Istanbul, Turkey.

Jackson, T. J., et al. (1995), Large area mapping of soil moisture using the ESTAR passive microwave radiometer in Washita-92, *Remote Sens. Environ.*, *53*, 27–37.

Jackson, T. J., D. M. Le Vine, A. J. Griffis, D. C. Goodrich, T. J. Schmugge, C. T. Swift, and P. E. O'Neill (1993), Soil moisture and rainfall estimation over a semiarid environment with the ESTAR microwave radiometer, *IEEE Trans. Geosci. Remote Sens.*, *31*(4), 836–841.

Jackson, T. J., D. M. Le Vine, A. Y. Hsu, A. Oldak, P. J. Starks, C. T. Swift, J. D. Isham, and M. Haken (1999), Soil moisture mapping at region scales using microwave radiometry: The southern great plains hydrology experiment, *IEEE Trans. Geosci. Remote Sens.*, *37*(5), 2136–2151.

Jirousek, M., M. Peichl, H. Süß (2010), A microwave imaging spectrometer for security applications, Proc. of SPIE Defense & Security Symposium – Passive MMW Imaging Technology XIII, Orlando, Fla., 5–9 April.

Kainulainen, J., K. Rautiainen, and M. Hallikainen (2007), First 2-D interferometric radiometer imaging of the Earth from an aircraft, *IEEE Geosci. Remote Sens. Lett.*, *4*(2), 241–245.

Kainulainen, J., K. Rautiainen, J. Lemmetyinen, J. Seppänen, P. Sievinen, M. Takala, and M. Hallikainen (2011a), Experimental study on radiometric performance of synthetic aperture radiometer HUT-2D—Measurements of natural targets, *IEEE Trans. Geosci. Remote Sens.*, *49*(2), 814–826.

Kainulainen, J., K. Rautiainen, and M. Hallikainen (2011b), Lessons learned from HUT-2D L-band airborne demonstrator, paper presented at IEEE 2011 International Geoscience and Remote Sensing Symposium (IGARSS'11), Vancouver, Canada.

Kainulainen, J., K. Rautiainen, J. Lemmetyinen, M. Hallikainen, F. Martin-Porquaras, and M. Martin-Neira (2011c), Detection of a sea surface salinity gradient using datasets of airborne synthetic aperture radiometer HUT-2D and a GNSS-R instrument, *IEEE Trans. Geosci. Remote Sens.*, *49*(11), 4561–4571.

Kainulainen, J., A. Colliander, J. Closa, M. Martin-Neira, R. Oliva, G. Buenadicha, P. Rubiales Alcaine, A. Hakkarainen, and M. Hallikainen (2012), Radiometric performance of the SMOS reference radiometers—Assessment after one year of operation, *IEEE Trans. Geosci. Remote Sens.*, *50*(5), 1367–1383.

Kaleschke, L., X. Tian-Kunze, N. Maaß, M. Mäkynen, and M. Drusch (2012), Sea ice thickness retrieval from SMOS brightness temperatures during the arctic freeze-up period, *Geophys. Res. Lett.*, *39*, L05501, doi:10.1029/2012GL050916.

Kerr, Y. H. (1997), Ramses: Proposition de mission spatiale sur mini satellite au colloque de prospective du CNES (TAOB), Toulouse, CESBIO.

Kerr, Y. H. (1998), The SMOS mission: MIRAS on RAMSES. A proposal to the call for Earth explorer opportunity mission, Toulouse (F), CESBIO: 50.

Kerr, Y. H. (2007), Soil moisture from space: Where are we?, *Hydrogeol. J.*, *15*, 117–120.

Kerr, Y. H., and E. G. Njoku (1990), A semi empirical model for interpreting microwave emission from semi-arid land surfaces as seen from space, *IEEE Trans. Geosci. Remote Sens.*, *28*(3), 384–393.

Kerr, Y. H., E. Assad, J. P. Fréteaud, J. P. Lagouarde, and B. Seguin (1987), Estimation of evapotranspiration in the Sahelian zone by use of Meteosat and NOAA-AVHRR data, *Adv. Space Res.*, *7*(11), 161–164.

Kerr, Y. H., A. Chanzy, J. P. Wigneron, T. J. Schmugge, and L. Laguerre (1995), Requirements for assessing soil moisture from space in arid and semi arid areas, Soil moisture and ocean salinity (SMOS) measurement requirements and radiometer techniques. N. ESA, Pays-Bas. ESA WPP-87: 15-33.

Kerr, Y. H., et al. (2010), The SMOS mission: New tool for monitoring key elements of the global water cycle, *Proc. IEEE*, *98*(5), 666–687.

Kerr, Y. H., J. Font, M. Martin-Neira, and S. Mecklenburg (2012), Introduction to the special issue on the ESA's Soil Moisture and Ocean Salinity mission (SMOS)—Instrument performance and first results, *IEEE Trans. Geosci. Remote Sens.*, *50*(5), 1351–1353.

Kerr, Y. H. (1996), Optimal choice for MIRAS frequencies: Scientific requirements, Toulouse, CESBIO. Project MMS MIRAS N° CCM3.

Laursen, B., and N. Skou (1998), Synthetic aperture radiometry evaluated by a 2-channel demonstration model, *IEEE Trans. Geoscience Remote Sens.*, *36*(3), 822–832.

Laursen, B., H. M. Pedersen, and N. Skou (1995), The DTU synthetic aperture radiometer demonstration model, in *Microwave Radiometry and Remote Sensing of the Environment*, edited by D. Solimini, pp. 451–461, VSP Int. Science Publishers, Utrecht, The Netherlands.

Le Vine, D. M., and J. C. Good (1983), Aperture synthesis for microwave radiometers in space, NASA Tech. Memo. TM-85033, August.

Le Vine, D. M., and M. Haken (2003), *RFI at L-band in Synthetic Aperture Radiometers*, vol. 3, pp. 1742–1744, Proc. International Geoscience & Remote Sensing Symposium (IGARSS), Toulouse, France, July.

Le Vine, D. M., T. T. Wilheit, R. E. Murphy, and C. T. Swift (1989), A multifrequency microwave radiometer of the future, *IEEE Trans. Geosci. Remote Sens.*, *27*, 193–199.

Le Vine, D. M., A. J. Griffis, C. T. Swift, and T. J. Jackson (1994), ESTAR: A synthetic aperture microwave radiometer for remote sensing applications, *Proc. IEEE*, *82*(12), 1787–1801.

Le Vine, D. M. (1999), Synthetic aperture radiometer systems, *IEEE Trans. Microwave Theory Tech.*, *47*(12), 2238–2236.

Le Vine, D. M., M. Kao, R. W. Garvine, and T. Sanders (1988), Remote sensing of ocean salinity: Results from the Delaware coastal current experiment, *J. Atmos. Oceanic Technol.*, *15*, 1478–1484.

Le Vine, D. M., M. Kao, A. B. Tanner, C. T. Swift, and A. Girffis (1990), Initial results in the development of a synthetic aperture microwave radiometer, *IEEE Trans. Geosci. Remote Sens.*, *28*, 614–619.

Le Vine, D. M., C. T. Swift, and M. Haken (2001a), Development of the synthetic aperture microwave radiometer, ESTAR, *IEEE Trans. Geosci. Remote Sens.*, *39*(1), 199–202.

Le Vine, D. M., T. J. Jackson, C. T. Swift, M. Haken, and S. W. Bidwell (2001b), ESTAR measurements during the Southern Great Plains experiments (SGP99), *IEEE Trans. Geosci. Remote Sens.*, *39*(8), 1680–1685.

Le Vine, D. M., G. S. E. Lagerloef, F. R. Colomb, S. H. Yueh, and F. A. Pellerano (2007a), Aquarius: An instrument to monitor sea surface salinity from space, *IEEE Trans. Geosci. Remote Sens.*, *45*(7), 2040–2050.

Le Vine, D. M., T. J. Jackson, and M. Haken (2007b), Initial images of the synthetic aperture radiometer 2D-STAR, *IEEE Trans. Geosci. Remote Sens.*, *45*(11), 3623–3632.

Le Vine, D. M., G. S. E. Lagerloef, and S. E. Torrusio (2010), Aquarius and remote sensing of sea surface salinity from space, *Proc. IEEE*, *98*(5), 688–703.

Lemmetyinen, J., et al. (2007), SMOS calibration subsystem, *IEEE Trans. Geosci. Remote Sens.*, *45*(11), 3691–3700.

Liu, H., J. Wu, S. Ban, J. Lu, J. Yan, S. Zhu, S. Zheng, C. Jiang, Q. Wu (2004), The CAS airborne X-band synthetic aperture radiometer: System configuration and experimental results International Geoscience and Remote Sensing Symposium, Anchorage, Proceedings of IGARSS'04, pp. 2230–2233.

Magagi, R. D., and Y. H. Kerr (1997a), Characterization of surface parameters over arid and semi-arid areas by use of ERS-1 wind scatterometer, *Remote Sens. Rev.*, *15*, 133–155.

Magagi, R. D., and Y. H. Kerr (1997b), Retrieval of soil moisture and vegetation characteristics by use of ERS-1 wind scatterometer over arid and semi-arid areas, *J. Hydrol.*, *189*(1–4), 361–384.

Magagi, R. D., and Y. H. Kerr (2001), Estimating surface soil moisture and soil roughness over semiarid areas from the use of the copolarization ratio, *Remote Sens. Environ.*, *75*, 432–445.

Martín-Neira, M. (1993), *MIRAS: A Two-Dimensional Passive Aperture Synthesis Radiometer, PIERS'93*, JPL.

Martín-Neira, M., and J. M. Goutoule (1997), MIRAS—A two-dimensional aperture-synthesis radiometer for soil moisture and ocean salinity observations, ESA Bulletin, No.92, pp. 95–104, November 1997, ESTEC, The Netherlands.

Martín-Neira, M., et al. (2002), MIRAS Demonstrator Pilot Project: Towards SMOS, ESA Bulletin 111, pp. 123–131, ESTEC, The Netherlands.
Martín-Neira, M., M. Suess, J. Kainulainen, and F. Martín-Porqueras (2008), The flat target transformation, *IEEE Trans. Geosci. Remote Sens.*, *46*(3), pp. 613–620.
McMullan, K., M. Brown, M. Martín-Neira, W. Rits, S. Ekholm, J. Marti, and J. Lemanczyck (2008), SMOS—The Payload, *IEEE Trans. Geosci. Remote Sens.*, *46*(3), pp. 594–605.
Merlin, O., A. G. Chehbouni, Y. H. Kerr, E. G. Njoku, and D. Entekhabi (2005), A combined modeling and multi-spectral/multi-resolution remote sensing approach for disaggregation of surface soil moisture: Application to SMOS configuration, *IEEE Trans. Geosci. Remote Sens.*, *43*(7), 2036–2050.
Merlin, O., A. Al Bitar, J. P. Walker, and Y. Kerr (2010), An improved algorithm for disaggregating microwave-derived soil moisture based on red, near-infrared and thermal-infrared data, *Remote Sens. Environ.*, *114*(10), 2305–2316.
Merlin, O., C. Rudiger, A. Al Bitar, P. Richaume, J. P. Walker, and Y. H. Kerr (2012), Disaggregation of SMOS soil moisture in southeastern Australia, *IEEE Trans. Geosc. Remote Sens.*, *50*(5), 1556–1571.
Moran, M. S., D. C. Hymer, J. Qi, and Y. Kerr (1998), Radar imagery for precision crop and soil management, *Modern Agric.*, *2*(1), 21–23.
Moran, M. S., D. C. Hymer, J. G. Qi, and Y. Kerr (2002), Comparison of ERS-2 sar and LANDSAT TM imagery for monitoring agricultural crop and soil conditions, *Remote Sens. Environ.*, *79*(2-3), 243–252.
Njoku, E., and J. A. Kong (1977), Theory for passive microwave remote sensing of near surface soil moisture, *J. Geophys. Res.*, *82*, 3108–3118, doi:10.1029/JB082i020p03108.
Peichl, M., and H. Süß (2005), Error analysis of sparse passive synthesis radiometers on UAV platforms, Proc. of SPIE Defense and Security Symposium 2005 – Passive MMW Imaging Technology VIII, Orlando, Fla., 28 March–1 April.
Peichl, M., H. Süß, W. Keydel (1996), First results of investigations on the use of microwave radiometers for detection and location of antipersonal mines, EUREL International Conference on "The Detection of Abandoned Land Mines," Conference Publication Number 431, ISBN 0852966695, ISSN 0537-9989, OREGA Print and Design, Great Britain.
Peichl, M., H. Süß, M. Süß, and S. Kern (1998), Microwave imaging of the brightness temperature distribution of extended areas in the near and far field using two-dimensional aperture synthesis with high spatial resolution, *Radio Sci.*, *33*(3), 781–801, doi:10.1029/97RS02398.
Peichl, M., M. Greiner, H. Süß (2000), *DLR Activities on Aperture Synthesis Radiometry*, International Geoscience and Remote Sensing Symposium IGARSS 2000, Honolulu, Hawaii, 24–28 July.
Peichl, M., S. Dill, H. Süß (2001), Advanced detection of anti-personnel landmines using multi-spectral low-frequency microwave radiometry techniques, in *Proceedings of the Progress in Electromagnetic Research Symposium PIERS 2001*, Osaka, Japan, 18–22 July.
Peichl, M., V. Wittmann, E. Anterrieu, B. Picard, N. Skou, S. Sobjaerg (2005), Final report: Scientific inputs for the SMOS level 1 processor development, ESA contract No. 17312/03/NL/FF, 16 February 2005 (1st version), 15 July.
Peichl, M., S. Dill, M. Jirousek, D. Berthel, H. Suess (2007), Passive microwave remote sensing for security applications, in *Proceedings of the 37th European Microwave Conference 2007 EuMC07*, Munich, Germany, 9–12 Oct.
Piles, M., A. Camps, M. Vall-llossera, I. Corbella, R. Panciera, C. Rudiger, Y. H. Kerr, and J. Walker (2011), Downscaling SMOS-derived soil moisture using MODIS visible/infrared data, *IEEE Trans. Geosci. Remote Sens.*, *49*(9), 3156–3166.
Raju, S., A. Chanzy, J. P. Wigneron, J. C. Calvet, Y. H. Kerr, and L. Laguerre (1995), Soil moisture and temperature profile effects on microwave emission at low frequencies, *Remote Sens. Environ.*, *54*, 85–97.
Rautiainen, K., J. Kainulainen, T. Auer, J. Pihlflyckt, J. Kettunen, and M. Hallikainen (2008), Helsinki University of Technology L-band airborne synthetic aperture radiometer, *IEEE Trans. Geosci. Remote Sens.*, *46*(3), 717–726.
Schmugge, T. J., and B. J. Choudhury (1981), A comparison of radiative-transfer models for predicting the microwave emission from soils, *Radio Sci.*, *16*(5), 927–938.
Schmugge, T. J., T. J. Jackson, and H. L. McKim (1980), Survey of methods for soil-moisture determination, *Water Resour. Res.*, *16*(6), 961–979.
Schmugge, T., P. Gloersen, T. T. Wilheit, and F. Geiger (1974), Remote sensing of soil moisture with microwave radiometers, *J. Geophys. Res.*, *79*(2), 317–323, doi:10.1029/JB079i002p00317.
Schreiber, E., M. Peichl, H. Süß (2010), Status of VESAS—A fully-electronic microwave imaging radiometer system, Proc. of SPIE Defense & Security Symposium – Passive MMW Imaging Technology XIII, Orlando, Fla., 5–9 April.
Skou, N. (1991), Workshop on "Advanced Microwave Radiometric Techniques", Final Report of ESTEC Contract No.8968/90/NL/US(SC), vol. 3 of 3, R 476, August.
Skou, N., and D. Le Vine (2006), *Microwave Radiometer Systems*, chap. 15, 2nd ed., Artech House, Norwood, MA.
Swift, C. T., D. M. Le Vine, and C. S. Ruf (1991), Aperture synthesis concepts in microwave remote sensing of the Earth, *IEEE Trans. Microwave Theory Tech.*, *39*(12), 1931–1935.
Thibaut, P. (1994), Etude d'un radiomètre imageur à synthèse d'ouverture et traitement du signal interférométrique, PhD, Institut National Polytechnique de Toulouse.
Thibaut, P., and Y. H. Kerr (1990), *Application of Aperture Synthesis in Passive Microware Remote Sensing*, Int Union of Radio Science, Hyannis, Mass.
Thibaut, P., Y. H. Kerr, B. Le Stradic, J. C. Magnan, M. Avignon, and F. Castanie (1990), Generation of a high resolution microwave brightness, Temperature map for assessing aperture synthesis radiometer performances. IGARSS'90, Md.
Thompson, A. R., J. M. Moran, and G. W. Swenson (2004), *Interferometry and Synthesis in Radio Astronomy*, Wiley-VCH Verlag, Weinheim, Germany.
Tsang, L., I. S. Koh, T. H. Liao, S. W. Huang, X. L. Xu, E. G. Njoku, and Y. H. Kerr (2013), Active and passive vegetated surface models with rough surface boundary conditions from NMM3D, *IEEE J. Selected Topics Appl. Earth Observations Remote Sens.*, *6*(3), 1698–1709.
Valencia, E., A. Camps, N. Rodriguez-Alvarez, I. Ramos-Perez, X. Bosch-Lluis, and H. Park (2011), Improving the accuracy of sea surface salinity retrieval using GNSS-R data to correct the sea state effect, *Radio Sci.*, *46*, RS0C02, doi:10.1029/2011RS004688.
Wagner, W., G. Bloschl, P. Pampaloni, J. C. Calvet, B. Bizzarri, J. P. Wigneron, and Y. Kerr (2007), Operational readiness of microwave remote sensing of soil moisture for hydrologic applications, *Nord. Hydrol.*, *38*(1), 1–20.
Waldteufel, P., J. Boutin, and Y. Kerr (2003), Selecting an optimal configuration for the soil moisture and ocean salinity mission, *Radio Sci. 38*(3), 8051, doi:10.1029/2002RS002744.
Wigneron, J. P., Y. H. Kerr, A. Chanzy, and Y. Q. Jin (1993), Inversion of surface parameters from passive microwave measurements over a soybean field, *Remote Sens. Environ.*, *46*, 61–72.
Wigneron, J. P., et al. (2007), L-band Microwave Emission of the Biosphere (L-MEB) model: Description and calibration against experimental data sets over crop fields, *Remote Sens. Environ.*, *107*, 639–655.
Wu, J., C. Zhang, H. Liu, W. Sun, and J. Yan (2007), *Clock Scan of Imaging Interferometric Radiometer and its Applications*, pp. 5244 –5246, Geoscience and Remote Sensing Symposium, 2007. IGARSS 2007, 23–28 July, Barcelona, Spain.
Wu, J., W. Sun, J. Zheng, C. Zhang, H. Liu, J. Yan, C. Wang, C. Wang, and S. Wang (2011), Imaging interplanetary CMEs at radio frequency from solar polar orbit, *Adv. Space Res.*, *48*(5), 943–954.

Yueh, S. H. (2000), Estimates of Faraday rotation with passive microwave polarimetry for microwave remote sensing of Earth surfaces, *IEEE Trans. Geosci. Remote Sens.*, *38*(5), 2434–2438, doi:10.1109/36.868900.

Zhang, C., H. Ohang, J. Wu, S. Zhang, J. Yan, W. Sun, and H. Li (2012), Imaging performance analysis for the Geostationary Interferometric Microwave Sounder (GIMS) demonstrator, Proc. of MicroRad, pp. 1–4. Italy, 5–9 March.

Zhang, S., J. Wu, J. Li, S. Zheng, J. Jiang (2002), Experiment results of synthetic aperture microwave radiometer International Geoscience and Remote Sensing Symposium, Toronto, Canada, Proceedings of IGARSS'02, pp. 3635–3637.

Zine, S., et al. (2008), Overview of the SMOS sea surface salinity prototype processor, *IEEE Trans. Geosci. Remote Sens.*, *46*(3), 621–645.

Zurita, A. M., I. Corbella, M. Martin-Neira, M. A. Plaza, F. Torres, and F. J. Benito (2013), Towards a SMOS Operational Mission: SMOSOps-Hexagonal, *IEEE Journal of Selected Topics in Applied Earth Observations and Remote Sensing, 6*(3), pp. 1769–1780.